SUPERCONDUCTING ACCELERATOR MAGNET DESIGN

S. Wolff
DESY, Hamburg, Germany

Abstract
Superconducting dipoles, quadrupoles and correction magnets are necessary to achieve the high magnetic fields required for big accelerators presently in construction or in the design phase. Different designs of superconducting accelerator magnets are described and the designs chosen at the big accelerator laboratories are presented. The most frequently used cosθ coil configuration is discussed in detail. Approaches for calculating the magnetic field quality including coil end fields are presented. Design details of the cables, coils, mechanical structures, yokes, helium vessels and cryostats including thermal radiation shields and support structures used in superconducting magnets are given. Necessary material properties are mentioned. Finally, the main results of magnetic field measurements and quench statistics are presented.

1. INTRODUCTION

Superconducting accelerator magnets are being used world-wide in the new generation of big particle accelerators. The goal of higher and higher energies in synchrotrons and storage rings can be reached only if the bending fields or the diameters of these rings, or even both, are increased to the upper limits. Sometimes ring diameters are limited by local boundary conditions or even by the fact that existing tunnels should be used. In this case increasing the magnetic fields is the only way to reach higher energies. In standard normal conducting magnets the field strength and quality are determined by the gap width and the shape of the magnetic steel poles. However, because of saturation already below 2.0 Tesla, the use of these magnets is rather limited. For higher fields yokeless magnets could be used but they are normally not economical due to their big volume and high energy consumption. Superconducting magnets are, therefore, the only reasonable solution to this problem in spite of their greater technical complexity.

A large series of superconducting accelerator magnets was built for the TEVATRON at Fermilab from 1979 to 1980. Industrial mass production of such magnets occurred for the first time from 1988 to 1990 for HERA. Other accelerators under construction or in the planning phase making use of superconducting accelerator magnets are UNK at Serpukhov, RHIC at BNL, SSC in Texas and LHC at CERN.

2. SUPERCONDUCTING MAGNET CONFIGURATIONS

Superconductivity can be used in accelerator magnets to save electrical energy or to increase the field strength or to do both. Several different approaches have been made so far to reach the desired goals including:

Superferric Magnets:

These magnets have the same structure as standard normal conducting magnets. Only the coil is replaced by a superconducting one. Magnetic steel yokes are still used to determine the field quality (Fig. 1 a). The yoke is cooled down to liquid helium temperature.

Window Frame Magnets:

The yoke has the form of a rectangular box in which the superconducing coils cover two sides. The iron poles are further away from the magnetic centre. Saturation effects are still big. Correction coils are usually required to compensate for field distortions at high currents (Fig.1 b).

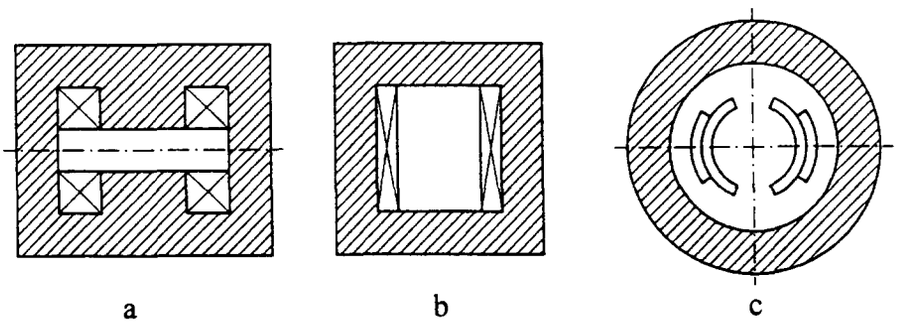

Fig. 1 Superconducting magnet configurations. Superferric (a),window frame (b) and cosθ approximation (c) magnets.

Cosθ Approximation Magnets:

The yoke, if existing at all, is far away from the magnet centre. The field quality is determined by the position of current carrying elements arranged in blocks or shells (Fig.1c).

All three approaches have been realised for building accelerator magnets. The one most commonly used today is the cosθ approximation type. It allows high fields to be reached with the most economic use of the very expensive superconducting material.

A coil consists of a long straight section and of coil ends of the race track or saddle type (Fig. 2).

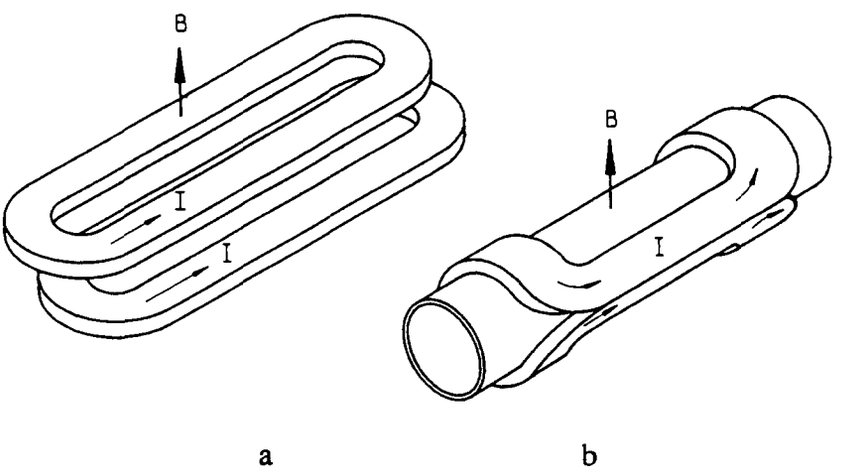

Fig. 2 Coil types. Race track (a) and saddle shape type (b).

3. FIELD ANALYSIS

Field quality plays an important role in accelerator magnets. Pure dipole fields are used for bending purposes, i.e. keeping the accelerated particles on a circular track. Quadrupole fields are used for focusing particle beams. Sextupole fields are needed for chromaticity corrections.

Field distortions lead to beam perturbations. The aim, therefore, is to build magnets with very high field quality. This means that only the desired pole is present and that distortions of this pole are as small as possible.

3.1 Field Representation

A convenient method to describe the field quality is a Fourier series representation in a polar co-ordinate system. The azimuthal field B_θ and radial field B_r around an axis of symmetry (Fig. 3) are then

$$B_\theta = B_{main} \sum_{n=1}^{\infty} \left(\frac{r}{r_0} \right)^{n-1} \left(b_n \cos n\theta + a_n \sin n\theta \right) \tag{1}$$

$$B_r = B_{main} \sum_{n=1}^{\infty} \left(\frac{r}{r_0} \right)^{n-1} \left(-a_n \cos n\theta + b_n \sin n\theta \right) \tag{2}$$

with r_0 = reference radius at which the field distortions are compared, B_{main} = main pole field, n = harmonic number. The harmonic coefficients b_n and a_n are called "normal" (b_n) and "skew" (a_n). In an ideal dipole for instance B_{main} is the field on the axis in vertical direction, b_1 = 1 and all other harmonics are equal to zero. In an ideal quadrupole B_{max} is the maximum field at $r = r_0$, b_2= 1 and all other harmonics are zero.

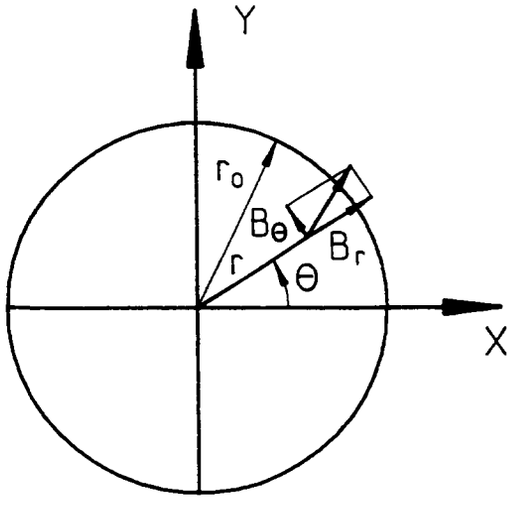

Fig. 3 Definitions for field representation

Magnets with main m pole symmetry normally have $b_n \neq 0$ for harmonic numbers

$n = (1 + 2k)m$, $k = 1, 2, 3 \ldots$

(i.e. for m = 1 (dipole), n = 3, 5, 7 ...and for m = 2 (quadrupole), n = 6, 10, 14).

Real magnets have all kinds of harmonic coefficients, also of the skew type (a_n) because of symmetry distortions.

3.2 Field Calculations

For field calculations elaborate computer programs are available which consume a lot of computer time if iron saturation is taken into account. For many applications where iron saturation can be neglected simpler analytic methods give much faster results.

3.2.1 Field of Current Carrying Wires

In a two-dimensional problem where a current I_i is entering into the plane at a location described by the radius r_i and the angle ϕ_i (Fig. 4) the z-component of the vector potential at a point P(r, θ) with $r < r_i$ is [1]

$$A_{z_i}(r,\theta) = \frac{\mu_0 I_i}{2\pi} \sum_{n=1}^{\infty} \frac{1}{n} \left(\frac{r}{r_i} \right)^n \cos(n(\phi_i - \theta)) \tag{3}$$

with μ_0 = magnetic permeability in air.

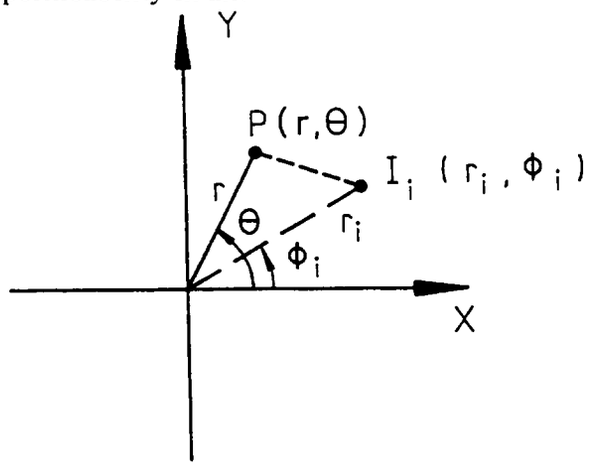

Fig. 4 Definitions for field calculations

Because of

$$B_{\theta_i} = -\frac{\partial A_{z_i}}{\partial r}, B_{r_i} = \frac{1}{r} \frac{\partial A_{z_i}}{\partial \theta} \tag{4}$$

we get

$$\begin{aligned} B_{\theta_i} &= -\frac{\mu_0 I_i}{2\pi r_i} \sum_{n=1}^{\infty} \left(\frac{r}{r_0} \right)^{n-1} \cos(n(\phi_i - \theta)) \\ &= -\frac{\mu_0 I_i}{2\pi r_i} \sum_{n=1}^{\infty} \left(\frac{r}{r_0} \right)^{n-1} (\cos n\phi_i \cos n\theta + \sin n\phi_i \sin n\theta) \end{aligned} \tag{5}$$

and with Eq. (1)

$$b_{n_i} = \left(\frac{r_o}{r_i}\right)^{n-1} \cos n\phi_i \tag{6}$$

$$a_{n_i} = \left(\frac{r_o}{r_i}\right)^{n-1} \sin n\phi_i . \tag{7}$$

If there are m wires, the field of the individual wires is superposed. Therefore, we get

$$B_\theta = \sum_{i=1}^{m} B_{\theta_i} \tag{8}$$

$$= -\frac{\mu_o}{2\pi} \sum_{i=1}^{m} \frac{I_i}{r_i} \sum_{n=1}^{\infty} \left(\frac{r}{r_i}\right)^{n-1} (\cos n\phi_i \cos n\phi + \sin n\phi_i \sin n\theta).$$

As the main pole of order p at a reference radius r_0 is given by

$$B_{main} = -\frac{\mu_o}{2\pi} \sum_{i=1}^{m} \left(\frac{I_i}{r_i}\right)\left(\frac{r_o}{r_i}\right)^{p-1} \cos p\phi_i \tag{9}$$

we get

$$b_n = \frac{\sum_{i=1}^{m} \frac{I_i}{r_i}\left(\frac{r_o}{r_i}\right)^{n-1} \cos n\phi_i}{\sum_{i=1}^{m} \frac{I_i}{r_i}\left(\frac{r_o}{r_i}\right)^{p-1} \cos p\phi_i} \tag{10}$$

$$a_n = \frac{\sum_{i=1}^{m} \frac{I_i}{r_i}\left(\frac{r_o}{r_i}\right)^{n-1} \sin n\phi_i}{\sum_{i=1}^{m} \frac{I_i}{r_i}\left(\frac{r_o}{r_i}\right)^{p-1} \cos p\phi_i}. \tag{11}$$

3.2.2 Field of Current Distribution

Assuming the current carrying elements are all at a constant radius "a" (Fig. 5) with the current varying according to a simple function

$$I(\phi) = I_0 \cos p\phi \tag{12}$$

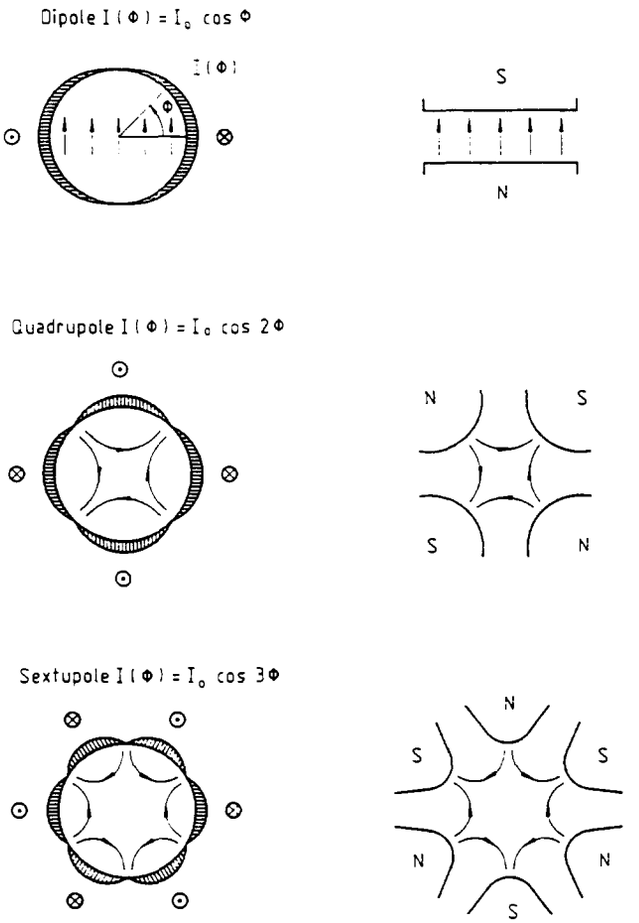

Fig. 5 Current distributions for pure dipole, quadrupole, and sextupole. On the right side the equivalent iron pole shapes are shown [2]

integration of Eq. (3) gives [2]

$$A_z(r,\theta) = \frac{\mu_0 I_0}{2}\frac{1}{p}\left(\frac{r}{a}\right)^p \cos p\theta \tag{13}$$

and, therefore, a pure field of order p

$$B_\theta = -\frac{\mu_0 I_0}{2a}\left(\frac{r}{a}\right)^{p-1} \cos p\theta \tag{14}$$

$$B_r = -\frac{\mu_0 I_0}{2a}\left(\frac{r}{a}\right)^{p-1} \sin p\theta. \tag{15}$$

Because of

$$B_x = B_r \cos\theta - B_\theta \sin\theta \tag{16}$$

and

$$B_y = B_r \sin\theta + B_\theta \cos\theta \tag{17}$$

we get for a dipole

$$\begin{aligned} B_x &= 0 \\ B_y &= -\frac{\mu_0 I_0}{2a} \end{aligned} \tag{18}$$

for a quadrupole

$$\begin{aligned} B_x &= gy \\ B_y &= gx \end{aligned} \tag{19}$$

with

$$g = -\frac{\mu_0 I_0}{2a^2} \tag{20}$$

and for a sextupole

$$\begin{aligned} B_x &= g'xy \\ B_y &= \frac{1}{2} g'\left(x^2 - y^2\right) \end{aligned} \tag{21}$$

with

$$g' = -\frac{\mu_0 I_0}{a^3}. \tag{22}$$

3.2.3 Field of Intersecting Ellipse Current Distribution

Instead of having $\cos p\phi$ current distribution at a constant radius, we may have constant current density j at specific coil cross sections. Ideal field configurations are achieved by intersecting circles or ellipses (Fig. 6). For a dipole configuration the field is [3]

$$\begin{aligned} B_y &= -\frac{\mu_0 jsc}{(b+c)} \\ B_x &= 0 \end{aligned} \tag{23}$$

with s, b and c indicated in Fig. 6.

For intersecting circles Eq. (23) reduces to

$$B_y = -\frac{\mu_0 js}{2} \tag{24}$$

and is independent of the radius of the circles.

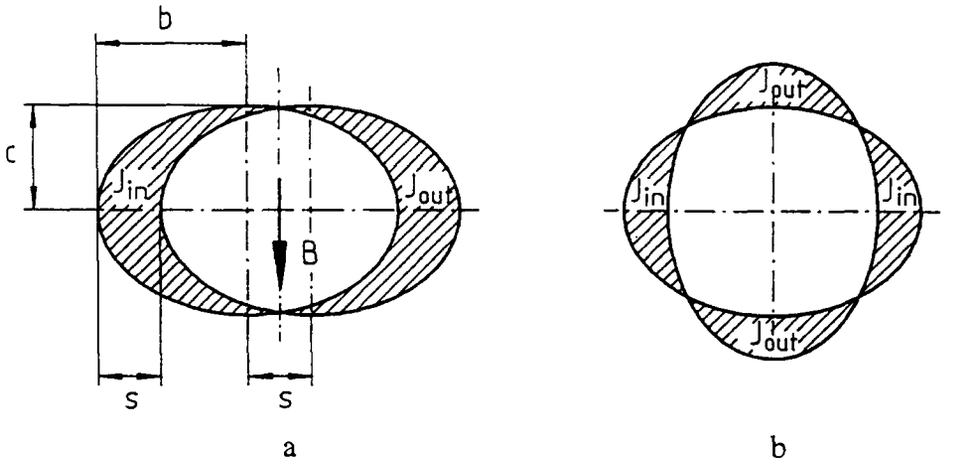

Fig. 6 Intersecting ellipses for dipole (a) and quadrupole (b) [3]

3.2.4 Approximation of Intersecting Ellipses

Filling the non-overlapping areas of intersecting ellipses with constant current density is not easy in practice. In order to simplify fabrication procedures, one would like to use not more than one or two different conductor types of round, rectangular or trapezoidal cross section. A convenient method, therefore, is to approximate the intersecting ellipses with blocks or azimuthal shells of conductors (Fig. 7).

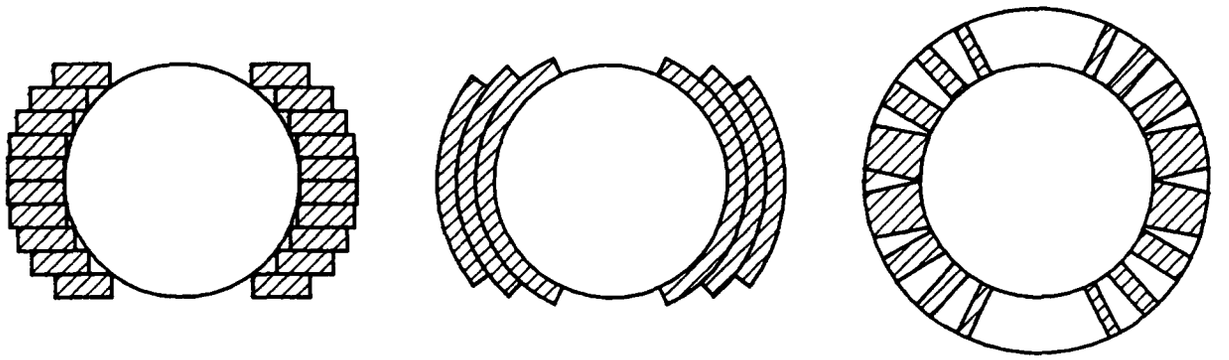

Fig. 7 Approximations of intersecting ellipses for dipoles

In a two-dimensional problem the z-component of the vector potential of an azimuthal current shell of radii a_1 and a_2, angle ϕ, pole symmetry p, and current density j is [1]

$$A_z(r,\theta) = \frac{\mu_0}{\pi} j \sum \frac{2pr^n \cos n\theta}{n^2} \sin n\phi \int_{a_1}^{a_2} \frac{da}{a^{n-1}} \tag{25}$$

for

$r < a_1$

with

$n = (2k + 1)p, \; k = 0, 1, 2, 3, \ldots$ (26)

Because of Eq. (4) we get

$$B_0 = \frac{2\mu_0}{\pi} j \frac{pr^{n-1}\cos n\theta}{n} \sin n\phi \int_{a_1}^{a_2} \frac{da}{a^{n-1}}. \tag{27}$$

For a dipole we have p = 1, k = 0,1,2,3 ... and, therefore, we get the dipole component (k = 0, n = 1)

$$B_{0_1} = -\frac{2\mu_0}{\pi} j \cos\theta \sin\phi (a_2 - a_1) \tag{28}$$

and the sextupole component (k = 1, n = 3)

$$B_{\theta_3} = \frac{2\mu_0}{3\pi} jr^2 \cos 3\theta \sin 3\phi \left(\frac{1}{a_2} - \frac{1}{a_1}\right). \tag{29}$$

The sextupole component is zero if $\phi = \pi/3$.
In this case the dipole strength is

$$B_{\theta_1} = -\frac{\sqrt{3}\mu_0}{\pi} j \cos\theta (a_2 - a_1). \tag{30}$$

3.2.5. Fields at Coil Ends

The calculation of the fields at the coil ends is more complicated and depends on the complexity of the current distributions. No analytic formulas exist. The simplest method is to approximate the conductors at the ends by a polygon and to apply Biot Savart's Law which gives a field vector at a point P

$$d\vec{B} = \frac{\mu_0}{4\pi} i \frac{d\vec{l} \times \vec{r}}{r^3} \tag{31}$$

for a current i flowing in direction $d\vec{l}$ with $\vec{r}$ being the vector from P to the starting point of dl.

The calculated fields in the whole space must then be subjected to a Fourier analysis. Another method is to cut the coil end into small sections in longitudinal (z) direction. This gives conductor cross sections in planes in which the field harmonics can be calculated in the same manner as in the straight sections. The whole end field is then obtained by integration (summation) over the z-direction. For up-down symmetric coil ends the z-component of the coil end field vanishes.

3.2.6 Iron Contribution to Field

Soft iron is used around superconducting coils for two purposes: to enhance the field at the coil centre and to reduce the stray field on the outside. For accurate field calculations programs are used which take into account a finite permeability μ and saturation effects. Such computer programs are for instance MAGNET, GFUN, POISSON, TOSCA, PROFI, MAFIA, ANSYS. Some of them are able to do three-dimensional calculations but may be difficult to use.

As saturation in superconducting magnets of the cosθ type starts at high currents only a much simpler calculation method can be used for quick analysis. In this case $\mu = \infty$ is assumed and the iron boundary is treated as an ideal mirror. The field on the axis is then obtained from a superposition of the fields from the real coils and from the image coils.

With a circular iron boundary of radius b we get the following parameters of the image currents (Fig. 8):

For individual wires (radii, angles and currents):

$$\begin{aligned} r_i' &= b^2 / r_i \\ \phi_i' &= \phi_i \\ I_i' &= I_i . \end{aligned} \tag{32}$$

For coil segments (radii, angle and current density):

$$\begin{aligned} a_1' &= b^2 / a_2 \\ a_2' &= b^2 / a_1 \\ \phi' &= \phi \\ j' &= j \frac{a_1^2 a_2^2}{b^4} . \end{aligned} \tag{33}$$

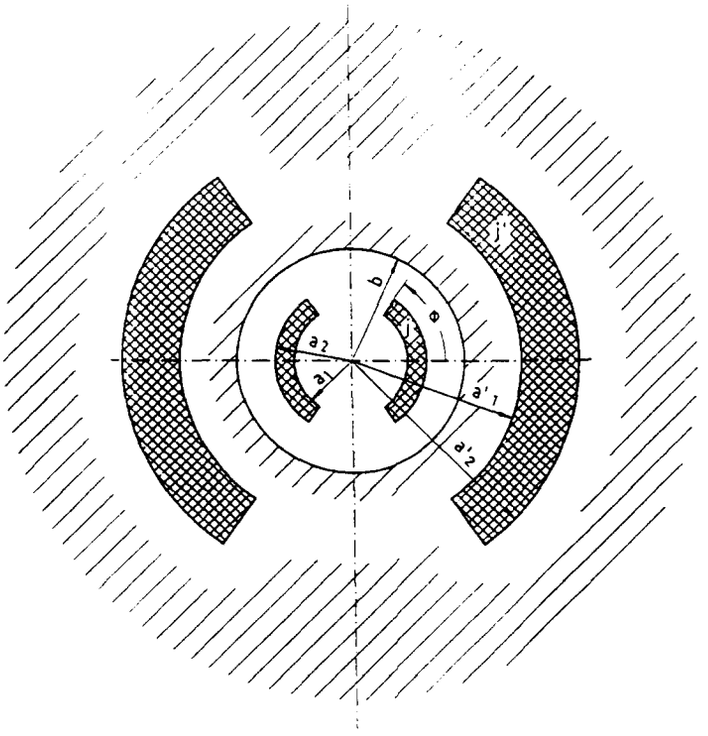

Fig. 8 Current images from a circular yoke boundary

The dipole field component for the coil segments of Section 3.2.4 and yoke radius b is, therefore,

$$B_\theta = -\frac{\sqrt{3}\mu_0}{\pi} j \cos\theta (a_2 - a_1)\left(1 + \frac{a_1 a_2}{b^2}\right). \tag{34}$$

3.2.7 Lorentz Forces

Forces play a big role in the design of superconducting magnets. Sudden cable motion of a few μm in a magnetic field will release magnetic energy which may be sufficient to introduce a transition to normal conductivity (quench). Therefore, the main concept of the design is that the conductor should not be able to move under magnetic forces. Big computer programs used for field calculation with iron saturation normally have subroutines which are able to calculate the forces also.

Simpler routines can, however, be used if iron saturation can be neglected. In case of individual wires - and each coil can be approximated this way - the forces in the straight section of length l are obtained simply by summation over individual force contributions between wire pairs.

$$F_x = \frac{\mu_0 l}{2\pi} \sum_i \sum_{k \neq i} \frac{I_i I_k (y_i - y_k)}{r_{ik}^2}$$
$$F_y = \frac{\mu_0 l}{2\pi} \sum_i \sum_{k \neq i} \frac{I_i I_k (x_i - x_k)}{r_{ik}^2} \tag{35}$$

where x_i, y_i describe the wire position in the coil cross section and r_{ik} are the distances between wires with index i and with index k.

4. EXAMPLES OF EXISTING MAGNET DESIGNS

For more than 10 years superconducting dipoles and quadrupoles have been designed for use in large accelerators.

The Tevatron dipole [4] at Fermilab was the first one built in large quantities (Fig. 9). It consists of a two-layer coil surrounded by laminated stainless steel collars inside a very narrow cryostat. The yoke is at room temperature. The support structure is relatively complicated as it has to take the forces between the yoke and the coil in case of asymmetry. Therefore, the heat load on the cryostat is rather high.

In the HERA dipole [5], [6], [7] (Fig. 10) the coil is clamped by laminated aluminium collars surrounded by the cold yoke. The support system consists of glass-fibre tapes and transversal rods. It is the first accelerator magnet built in large quantities by industry.

In the RHIC magnet [8] (Fig. 11) the one-layer coil is surrounded by the yoke without any collars. The necessary pre-compression of the coil is achieved by welding stainless steel half shells around the yoke.

For the SSC dipole [9] (Fig. 12), which has a two-layer coil, stainless steel collars and a cold yoke, a new support system consisting of posts of glass-fibre and carbon-fibre reinforced material has been developed. This leads to very low heat load. About 8000 magnets will have to be built by industry. A similar support system is now used for RHIC magnets.

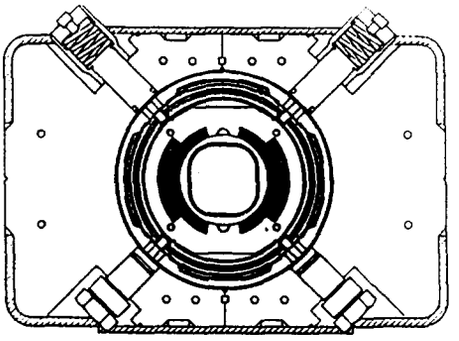

Fig. 9 Tevatron warm yoke dipole

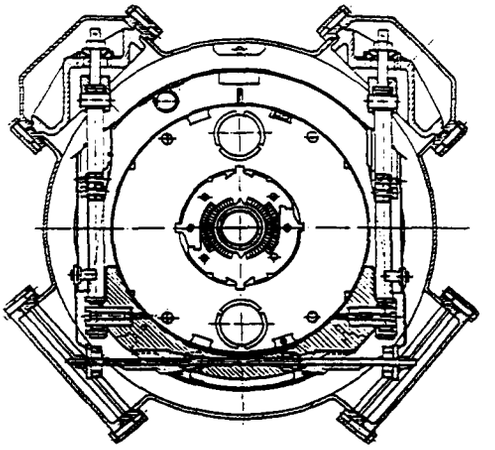

Fig. 10 HERA dipole

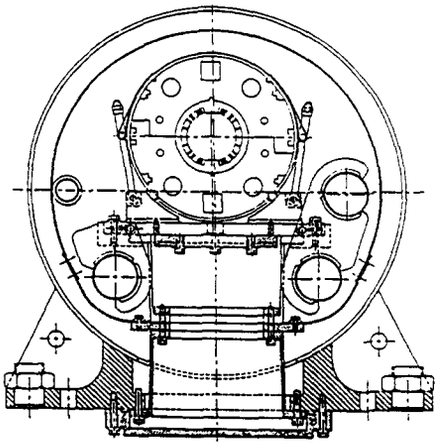

Fig. 11 RHIC dipole

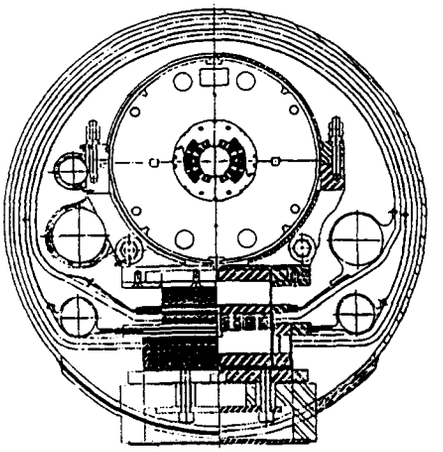

Fig. 12 SSC dipole

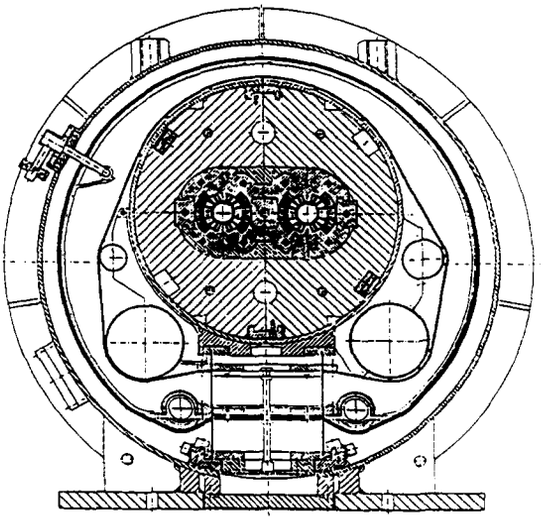

Fig. 13 LHC dipole

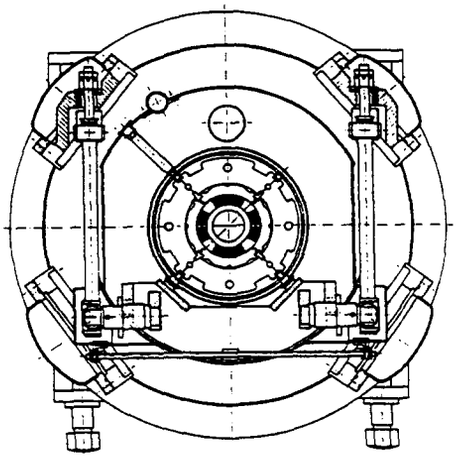

Fig. 14 HERA quadrupole

The LHC dipole [10] (Fig. 13) has two coils in one aluminium or stainless steel collar or in separate collars surrounded by a single yoke. An aluminium cylinder is used to achieve the necessary pre-compression. The support structure is similar to the one at the SSC or the RHIC magnet. The magnet will be cooled to 2 K in order to reach 10 T.

As an example of a quadrupole the HERA version [11] is shown in Fig. 14. It has a two-layer coil surrounded by laminated stainless steel collars and by a cold iron yoke. A special inertia tube made from stainless steel is used to assure a very accurate alignment of the magnet axis.

All these magnets are made using NbTi superconductor.

5. DESIGN DETAILS

After the overview of superconducting accelerator magnets, details of the design of individual magnet components are presented and discussed. For many of the details the HERA magnet [6], [7] is taken as the reference because it is the one which has been built in large quantities just recently. However, deviations in the design details are also discussed.

5.1 Superconducting Cable

The superconducting (SC) cable presently used in practically all accelerator magnets is a keystoned cable of the so-called Rutherford type. It is made from superconducting wires (strands), each containing many fine superconducting filaments embedded in a copper matrix (Fig. 15).

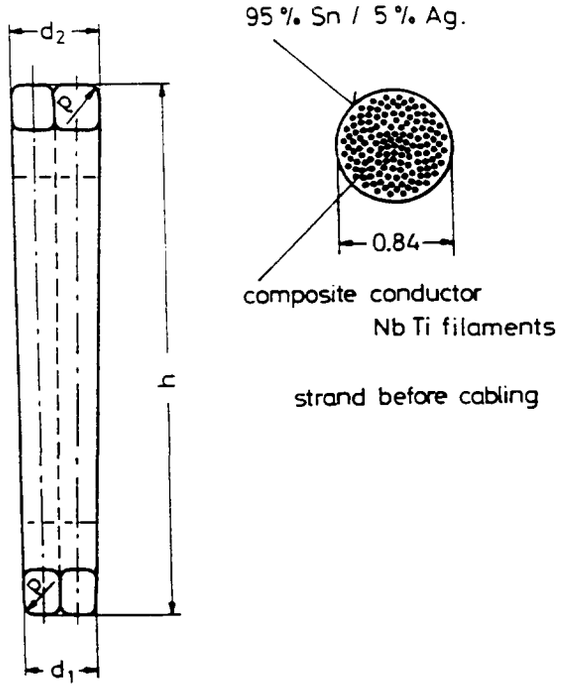

Fig. 15 HERA cable, d_1 = 1.28 mm, d_2 = 1.67 mm, ~ 1200 NbTi filaments of 14 μm diameter per strand, critical short sample current ≥ 8000 A at 4.6 K and 5.5 Tesla

5.1.1 Superconducting Wire

Important properties of the wire are the Cu/SC ratio which is between about 1.0 and 2.25 (RHIC), and the filament diameter which is less than 20 μm.

The superconductor normally is NbTi alloy (~47 weight% Ti). But also attempts to use Nb_3Sn have been made [12]. Copper is needed to protect the superconductor in the case of a quench since it is able to carry the current for the short time that the superconductor material is highly resistive. It is also used to remove heat which may be produced in a superconductor during flux jumps.

Fine filaments are necessary to stabilise the superconductor against flux jumps which may create sufficient heat for it to quench. The so-called dynamic stabilisation concept [3] leads to a filament diameter of < 50 μm for NbTi at 6 T and 4.2 K.

Stronger requirements for the filament diameter come from persistent current phenomena. During ramping of the field, shielding currents are induced in the filaments in order to keep the superconductor free of field (below H_{c1}). Nevertheless, in hard (Type II) superconductors field may even penetrate into the superconductor (between H_{c1} and H_{c2}) resulting in shielding currents also in the superconducting material (Fig. 16, [2]). This leads to field distortions at low fields, i.e. dipole, sextupole (Fig. 17), decapole etc., hysteresis in dipoles and quadrupole, 12-pole etc., hysteresis in quadrupoles [13].

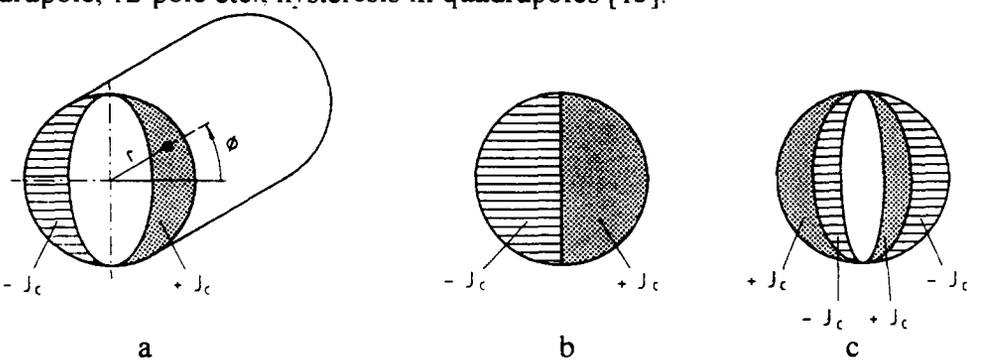

Fig. 16 Superconducting shielding currents at up-ramping (a), at full field penetration (b), at down-ramping (c).

This phenomenon can also be described as a magnetisation of the superconductor material. It is possible to calculate a peak magnetisation

$$M_p = \frac{4}{3\pi}\mu_0 j_c a \tag{36}$$

with a = filament radius and $j_C(B,T)$ = critical current density. This shows that the filament diameter $d_f = 2a$ should be kept small. Present technology uses wires with 5-6 μm thick NbTi filaments in the copper matrix. Further reduction of filament diameters leads to an increase of magnetisation due to proximity coupling. This could be avoided using CuMn as an interfilamentary matrix instead of copper. Filament magnetisation could also be avoided by ferromagnetic shielding achieved by either replacing a few NbTi filaments by Ni filaments or by NiCu plating of strands [14].

The filaments inside the copper matrix are twisted in order to avoid long eddy current loops in which the current may decay leading to a change of fields with time. For HERA cable the filament twist pitch is 25 mm.

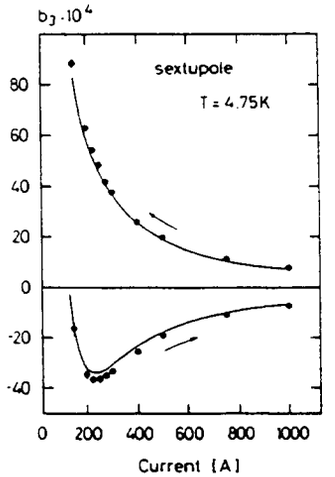

Fig. 17 Averaged sextupole coefficient with rms variations for 315 HERA dipoles as a function of current [13]. The solid curve is a model calculation.

The wires may be tinned in order to create a defined surface layer, to avoid corrosion and make soldering easier. For A.C. application the wires may be covered with an oxide layer in order to reduce eddy currents in the cable.

5.1.2 Cabling

The wires are cabled and keystoned to the desired shape given by the coil design. Important properties are the filling factor A_f, the keystone angle α_k and the compaction factor A_c. The filling factor is defined as:

$$A_f = \frac{n_s f_s}{F_c \cos\beta} \tag{37}$$

with n_S = number of strands in the cable

f_S = cross sectional area of strand

β = twist angle of cable

F_C = cross sectional area of cable.

The keystone angle is

$$\alpha_k = arctg\frac{d_2 - d_1}{h} \tag{38}$$

with d_1, d_2 inner and outer cable thickness, h = cable width.

The compaction factor is

$$A_c = \frac{d_1}{2d_s} \tag{39}$$

with d_S = strand diameter.

The values for the HERA cable are

$A_f = 0.93$, $\alpha_k = 2.33°$, $A_c = 0.76$.

As a high keystone angle bears the risk for degradation of the cable performance at the small edge more recent magnet designs have keystone angles only slightly above 1.0 (RHIC,

SSC and LHC). On the other hand keystone angles of up to 4.6° have been achieved at KEK, Japan without much degradation [15].

The cable corners must be round in order not to cut through the insulation.

The residual resistivity ratio (RRR) of resistances at 295 K (R_{295K}) and at 10 K (R_{10K})

$$RRR = \frac{R_{295K}}{R_{10K}} \tag{40}$$

is about 70 for HERA.

5.1.3 Cable Insulation

The requirements for the cable insulation are

- good electrical properties (i.e. high break-through voltage)
- good mechanical properties (i.e. elasticity, yield strength, also at liquid helium temperature)
- good resistivity against radiation damage (lifetime dose for HERA is ~ 5 x 10^6 Gray).

The type of insulation commonly used today is shown in Fig. 18 (for HERA).

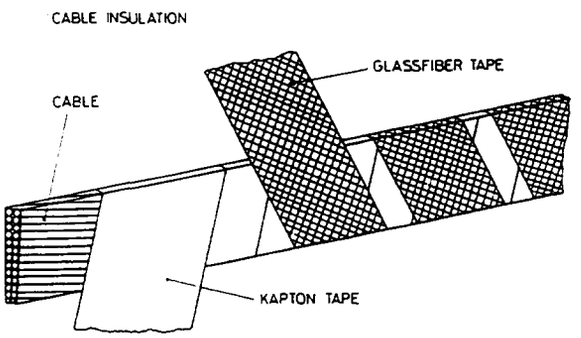

Fig. 18 Cable insulation

Although Kapton is a very good material for this purpose, it is difficult to use above 70 MPa compression at room temperature because it will start flowing under this load. The material is relatively sensitive to breaks and cut-throughs due to burrs and sharp edges. Therefore epoxy-impregnated glass-fibre tape is used to strengthen the insulation. Adhesive Kapton without glass-fibre tape has been tried for RHIC and SSC prototype magnets.

Before insulating, the cable is cleaned in an ultrasonic bath in order to remove dirt. During the insulation process a high voltage insulation test is performed (i.e. 1 kV, 1000 Hz).

5.2 Collared-Coil Design

The collared coil is probably the most critical part in the magnet. Therefore, the design and the manufacturing require special attention.

5.2.1 Straight Section Coil Design

Non-overlapping areas of overlapping circles or ellipses must be filled with conductor shells (see Section 3.2.4). Usually at least two shells are necessary in order to achieve the required field quality. Preliminary calculations can be made with uniform current density. The

shells are then segmented so that they can be filled with cable. Here the cable thickness and insulation thickness (in the fully compressed state) is important.

Coil layer angles are adjusted so that the field quality is optimised, i.e. all higher harmonic coefficients are $\leq 1 \times 10^{-4}$ at a reference radius of about 2/3 of the coil radius with the inner yoke radius chosen properly.

In order to avoid 14 and 18 poles wedges of copper or glass-fibre epoxy have to be put in. The HERA coil (Fig. 19) [6] may serve as an example for the obtained field quality given in Table 1.

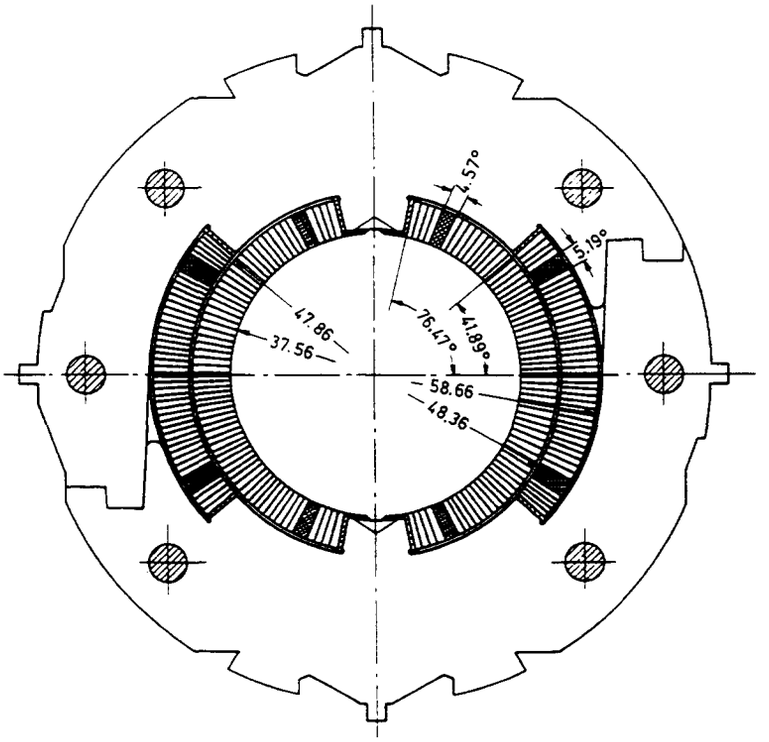

Fig. 19 HERA coil cross section

The accuracy of the coil angles and radii is limited, however, due to manufacturing errors. Such errors can be characterised by a set of transformations (Fig. 20) which result in harmonic changes (Table 2). The load line for this coil with yoke is shown in Fig. 21. The forces on individual cables are illustrated in Fig. 22.

In case of cable with a low keystone angle the angular space in the coil shell can not be filled uniformly. The coil wedges have a triangular or trapezoidal cross-section (RHIC, SSC, LHC).

The coil is carefully insulated on the outside using several layers of Kapton foil.

5.2.2 Coil Ends

Standard race track coils result in field enhancements at the innermost cable in the coil ends beyond the field maximum in the straight section. When a yoke is used this enhancement can be avoided if the yoke ends at or before the end of the straight section of the coil.

Table 1

Calculated harmonic coefficients at $r_0 = 2.5$ cm in a straight HERA dipole section, without iron saturation and persistent current effect

b_3	$0.0 \cdot 10^{-4}$
b_5	$0.9 \cdot 10^{-4}$
b_7	$0.3 \cdot 10^{-4}$
b_9	$-0.6 \cdot 10^{-4}$
b_{11}	$-0.1 \cdot 10^{-4}$
b_{13}	$-0.4 \cdot 10^{-4}$
b_{15}	$-0.3 \cdot 10^{-4}$

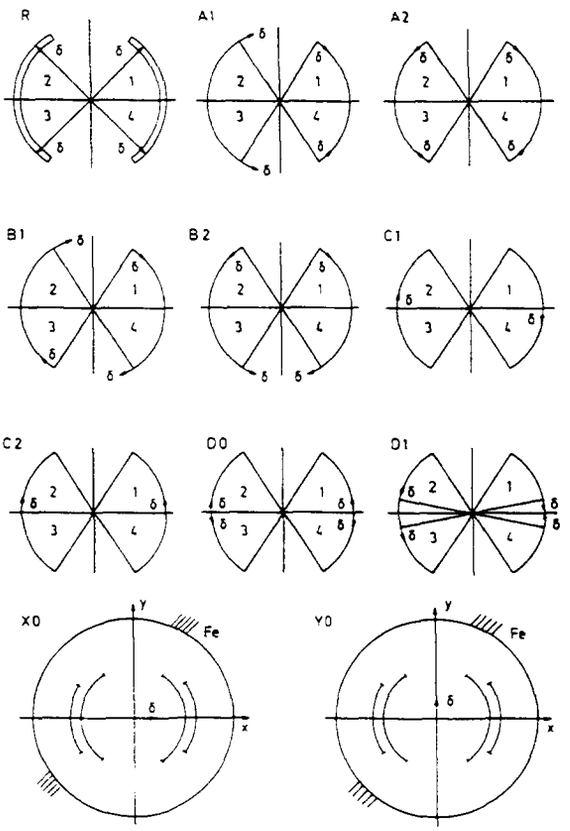

Fig. 20 Transformations needed to determine the influence of tolerances on harmonic coefficients (see Table 2)

Table 2

Effect of mechanical tolerances on harmonic coefficients at HERA dipole coil. The effect was calculated for transformations R, A1, A2, B1, B2, C1, C2, DO, D1, XO, YO illustrated in Fig. 20 at a radius $r_0 = 25$ mm. The amplitude of deformation was chosen to be $\delta = 0.1$ mm. Numbers in brackets are for a coil without yoke.

transfor-mation	n	inner coil	inner coil	outer coil	outer coil
		$10^{-4}a_n$	$10^{-4}b_n$	$10^{-4}a_n$	$10^{-4}b_n$
R	1		-9.0 (-14.6)		-3.5 (-7.1)
	3		2.2 (2.0)		-1.7 (-2.2)
A1	2		7.5 (9.1)		2.4 (2.7)
	4		-1.2 (-1.5)		0.9 (1.2)
A2	1		6.4 (6.8)		1.7 (1.6)
	3		2.4 (3.1)		1.7 (2.2)
	5		-1.1 (-1.4)		0.3 (0.4)
	7		0.3 (0.4)		- (-)
B1	1	-5.8 (-6.0)		-3.6 (-3.4)	
	3	4.3 (5.4)		-0.3 (-0.4)	
B2	2	1.2 (1.4)		-1.8 (-2.1)	
	4	2.3 (2.9)		0.3 (0.3)	
	6	-0.5 (-0.6)		0.2 (0.3)	
C1	1	-8.1 (-8.4)		-4.0 (-3.7)	
	3	-2.0 (-2.6)		-1.5 (-1.8)	
	5	- (-)		-0.3 (-0.4)	
C2	2	5.3 (6.5)		2.7 (3.1)	
	4	0.4 (0.4)		0.7 (0.9)	
D0	1		-3.7 (-3.7)		-0.8 (-0.8)
	3		-4.9 (-6.2)		-1.2 (-1.3)
	5		-1.6 (-2.0)		-0.5 (-0.6)
D1	2		5.7 (6.9)		1.3 (1.4)
	4		3.0 (3.8)		0.8 (1.0)
	6		0.8 (1.0)		0.3 (0.3)
X0 (complete coil) $10^{-4}b_2 = 1.5$ Y0 (complete coil) $10^{-4}a_2 = 1.3$					

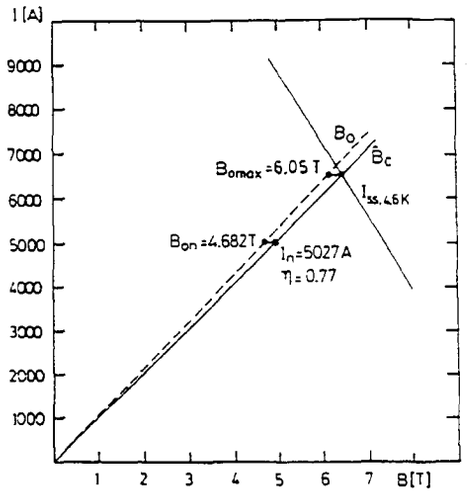

Fig. 21 HERA dipole load line, B_0= field on axis B_c = maximum field on conductor.

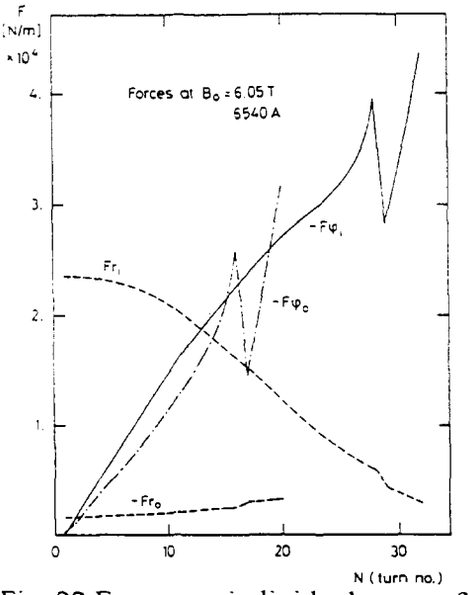

Fig. 22 Forces on individual turns of Hera coils

Standard race-track coils also result in higher harmonic coefficients at the coil ends, i.e. b_3 and b_5 in a dipole. This can be avoided by putting spacers between the turns. During coil winding the flat cable should not be deformed excessively by bending it over its small edge. This is achieved by arranging the cables in the coil ends of that kind that the cable edges have about the same perimeter. This leads to a flattening of the coil layer thickness in the coil ends. The coil end spacers can be designed to compensate for this flattening and to give additional support to the turns radially (SSC) [16].

As an example the HERA dipole inner layer coil end is shown (Fig. 23) and the sextupole harmonic coefficient in the end region (Fig. 24) [17]. The integral of this harmonic coefficient along the magnet axis cancels more or less.

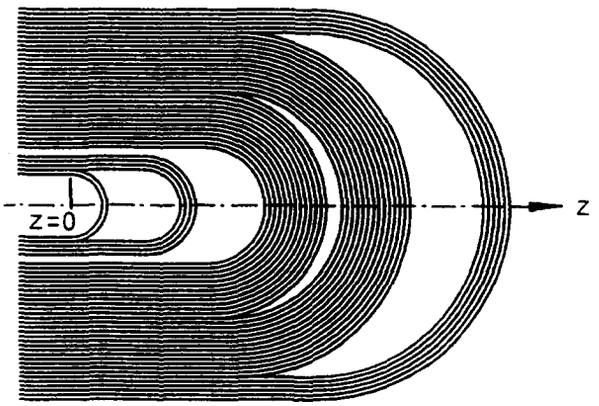

Fig. 23 HERA coil end, inner layer.

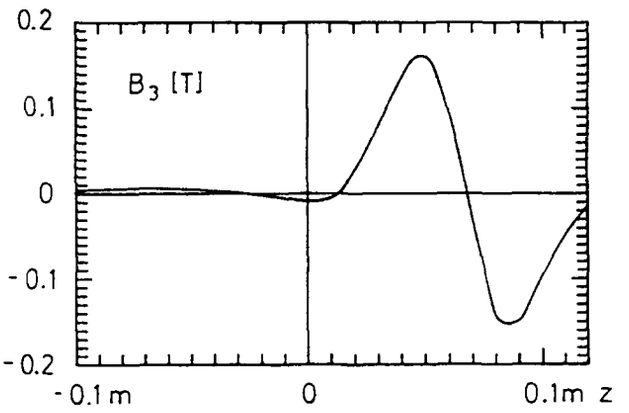

Fig. 24 Sextupole at HERA coil end, z = 0 at yoke end.

5.2.3 Collars

Magnetic (Lorentz) forces tend to disrupt the coil horizontally. They must be taken by a rigid mechanical structure. In order to avoid quenches introduced by coil motion, the coil must be held so tightly that the turns will not move when the coil is powered. The coil may be surrounded by the yoke directly (as at RHIC magnets [8]) but normally there are separate collars of non-magnetic material like stainless steel or aluminium alloy. If stainless steel is used, care must be taken that material can not become magnetic either by welding or by cold work (stamping) or during cool-down. Only a few steel types can be used (i.e. 316 LN, Nitronic 40, DIN standard steel 1.4429). But it is not sufficient to order just the right steel type. The chemical content (in %) is the important criterion. So-called δ-Ferrites can be present in steels. They are normally converted to austenite by annealing but can re-appear by cold work or welding. To determine the δ-Ferrite content, one can use the Schaeffler diagram (Fig. 25), in which the Ni equivalent promoting the austenite is plotted versus the Cr equivalent promoting the ferrite [18].

$$\text{Ni equivalent} = \text{Ni} + 0.11\ \text{Mn} - 0.0086\ \text{Mn}^2 + 18.4\ \text{N} + 24.5\ \text{C} \quad (41)$$

$$\text{Cr equivalent} = \text{Cr} + 1.21\ \text{Mo} + 0.48\ \text{Si} \quad (42)$$

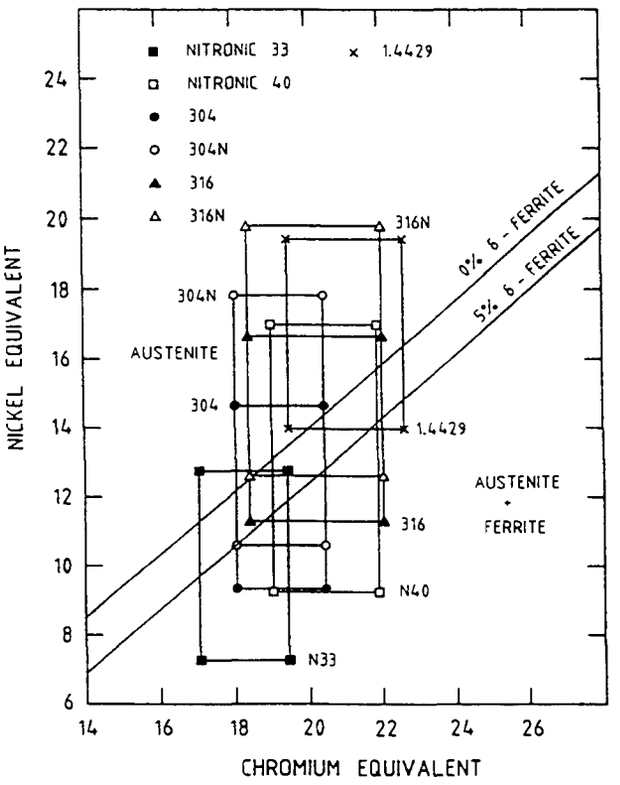

Fig. 25 Schaeffler diagram

Suitable steels should sit above the 0 % δ-Ferrite line. Steels below the 5 % δ-Ferrite line are questionable. In addition, Fe-Cr-Ni steels may transform to martensite at low temperature which also results in the appearance of ferromagnetic regions. The temperature M_S is defined as the one at which martensite forms in the absence of plastic deformations.

$$M_S(\pm 50\ K) = 1578 - 61.1\ Ni - 41.7\ Cr - 33.3\ Mn - 27.8\ Si - 1667\ (C + N) - 36.1\ Mo \quad (43)$$

This value should be around 0 or below. For plastic deformations martensite may already form at temperatures which are 300 - 400 K higher than M_S.

How a partly magnetic material may influence the field quality (main pole and higher harmonics) may be seen from a calculation for the HERA quadrupole magnet (Fig. 26, [19]).

Aluminium alloys are fully non-magnetic and, therefore, such an alloy has been used for the HERA dipole (Al Mg 4.5 Mn, G 35). Another advantage is that aluminium shrinks more than stainless steel during cool-down, practically in the same manner as the coil. Therefore, when using aluminium alloy no excessive pre-load (which is released during cool-down) is necessary. For instance, if stainless steel collars had been used the coil would have required about 12.5 % more pre-load at room temperature than is actually used at helium temperature.

The collars must be designed carefully because an optimum must be found. On the one hand they should be as thin as possible radially in order not to lose too much field contribution from the iron. On the other hand they must stand the mechanical and magnetic forces safely. For optimisation, finite element programs are commonly used which allow the areas of maximum stress to be investigated.

Keeping the coil ends under compression radially is difficult. For HERA magnets no attempt was made to achieve this. For the Fermilab design for SSC dipoles coil ends and collets are compressed radially by a tapered aluminium cylinder put in place hydraulically [16].

The tensile yield strengths of stainless steels and high strength aluminium alloys do not differ much at room temperature. The yield strength for DIN stainless steel 1.4429 is about 295 MPa compared to 270 MPa for the aluminium alloy used for HERA.

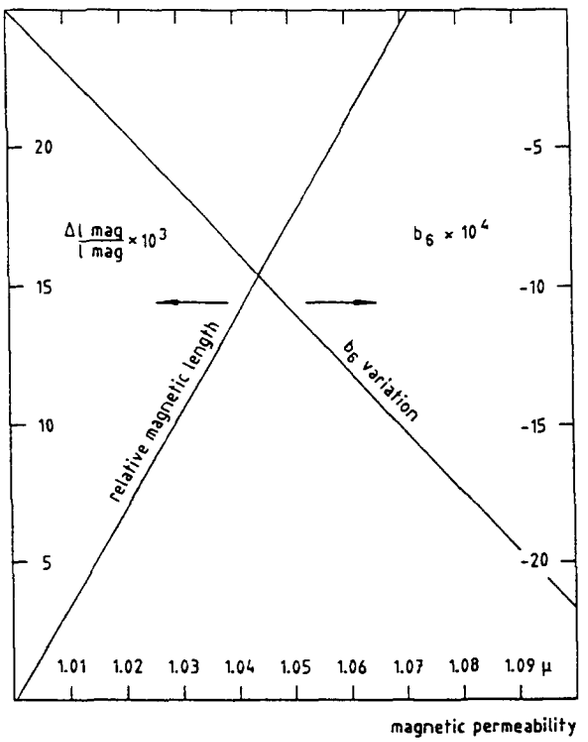

Fig. 26 Influence of magnetic permeability μ on field quality in HERA quadrupoles [19]

The collars are built up from laminations of thickness 1 - 4 mm. For aluminium alloy collars for HERA (4 mm thick) the "fine blanking" method was used.

There are different methods for locking the collars. Besides welding (TEVATRON), rods (HERA, LHC) or keys (SSC, UNK) are applied. Rods have the advantage that the stress distribution around them is optimal (Fig. 27) [20].

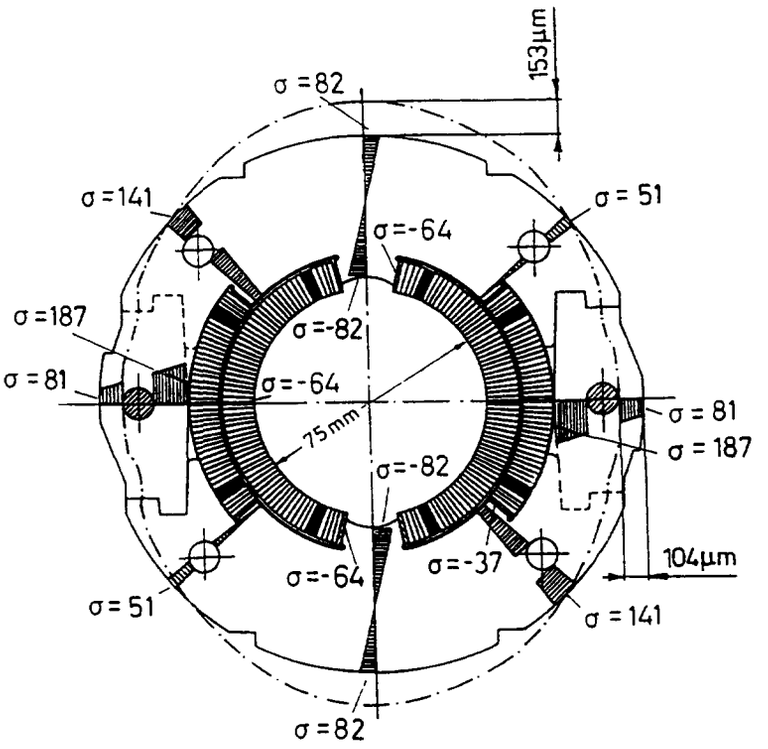

Fig. 27 Local stresses (σ [N/mm^2]) in HERA aluminium collars and elastic deformation at 4 K and zero current

During collaring of the HERA coil the coil is slightly over-compressed. Then the rods are inserted and the pressure is released. The compression of the coil during collaring, cool-down and current ramping has been measured on a 1 m HERA model magnet (Fig. 28). The measurement showed that due to the use of aluminium no decrease of compression occurs during cool-down [21].

Locking the coils with wedges near the horizontal plane requires less over-compression. Detailed measurements on the forces acting on the collars throughout collaring, cool-down, current ramp cycle and warm-up have been performed for SSC prototype magnets, showing that the coil is under compression from the collars during the whole current cycle [22].

RHIC magnets do not have collars at all. The coil is surrounded by an injection-moulded mineral-loaded glass phenolic spacer serving as insulation and creating a distance with respect to the surrounding carbon steel yoke [23].

5.3 Iron Yoke

The collared coil is surrounded by a laminated iron yoke. The material is a low-carbon steel with specified maximum coercive force and minimum inductance at given field values. A measured magnetisation curve for steel used at HERA magnets is given in Fig. 29. A histogram of the coercive force is shown in Fig. 30 [24].

Lamination thicknesses can be chosen to minimise cost, the fine blanking method being used for thick laminations (HERA: 5 mm). Changes of the permeability in the stamping region may occur but are not important for superconducting magnets, where the iron is far away from the region of interest. A vertical split of the half yokes is usually preferred.

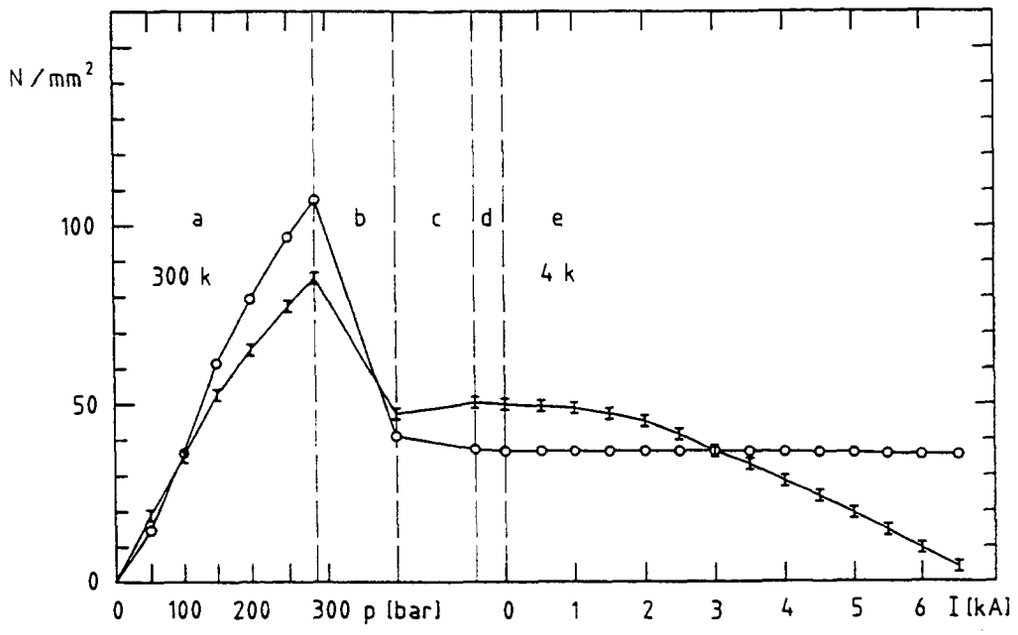

Fig. 28 Stress in the HERA coil during collaring (a) as a function of closing pressure in the press, external force release (b), cool down (c), stay at helium temperature (d), magnet powering as a function of current (e). Circles are for outer coil layer, bars for inner coil layer.

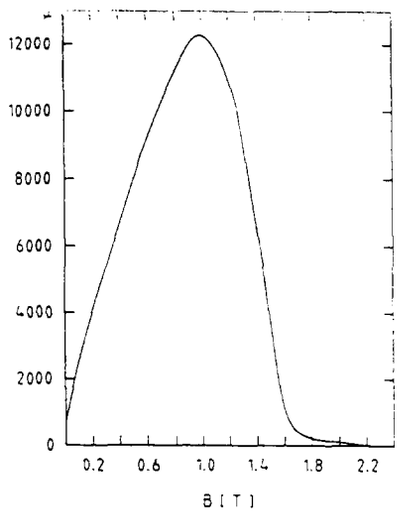

Fig. 29 Permeability of HERA yoke steel, annealed.

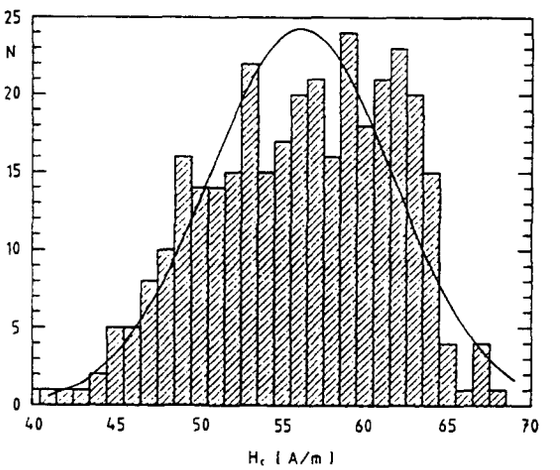

Fig. 30 Coercive force distribution of HERA yoke steel

The centring of the collared coil inside the yoke is achieved by keys at the collars fitting into grooves at the yoke. For the HERA dipoles bronze channels are used around the keys in order to avoid too much friction. The gaps between yoke and collars can be designed such that the yoke will take over the radial forces when the collars are loaded to their limits (Fig. 31), [7].

For the SSC dipoles the yoke tightly clamps the collars over most of their circumference. For the Fermilab design using a vertical yoke split this is achieved by a slight pro-ovalization of the collars horizontally. The BNL design has a horizontal yoke split which requires a slight vertical anti-ovalization to achieve a good line contact [25]. The half yokes are welded (HERA) or keyed (RHIC) together longitudinally or they are just clamped by the surrounding helium vessel. Thick stainless steel yoke endplates limit the yoke and coil ends.

The radial thickness of the yoke influences the saturation occurring at high currents (Fig. 32).

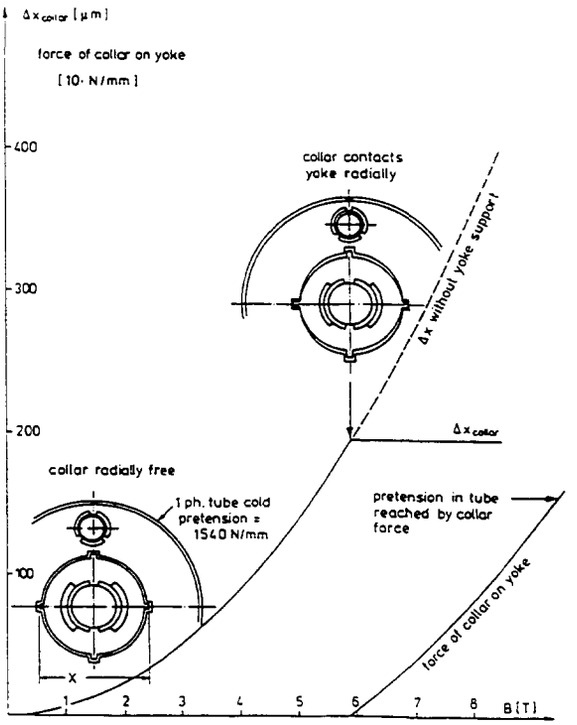

Fig. 31 Calculated deformation of collar and its force on yoke for HERA dipole [7]

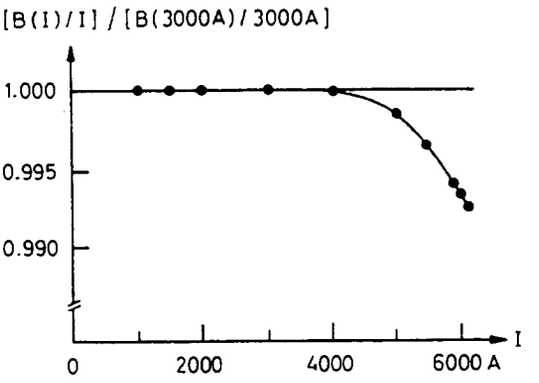

Fig. 32 Normalised central HERA dipole field as a function of current [17]

5.4 Electrical Connections

There may be splices in the coil which must be soldered with sufficient overlap (at least of the cable twist pitch length) that the resistance is small ($\sim 2 \times 10^{-9}$ Ω). Soldering is done without acid flux and with silver-tin (5 % silver) or lead-tin (40 % lead) solder.

At the coil ends and in the interconnection area the superconductor is reinforced with either copper braid - where flexibility is needed - or with solid copper of sufficient cross section. The cross section depends on the allowed maximum temperature T_{max} ("hot spot") and the time-constant τ for discharge of the system. Here the allowed $\int j^2 dt$ is important.

The temperature increase in a normal conductor due to Joule heating is

$$dT = \frac{1}{C(T)} \rho(T) j^2(t) dt \tag{44}$$

with C(T) = specific heat per unit volume, ρ(T) = specific electrical resistivity, and j = current density.

By separating the terms of independent variables one obtains

$$j^2(t)dt = \frac{C(T)}{\rho(T)}dT \tag{45}$$

and by integration

$$\int_0^\infty j^2(t)dt = \int_{T_0}^{T_{max}} \frac{C(T)}{\rho(T)}dT = f(T_{max}) \tag{46}$$

As the material properties as a function of temperature are known, this function can be calculated. For copper the curve given in Fig. 33 is obtained.

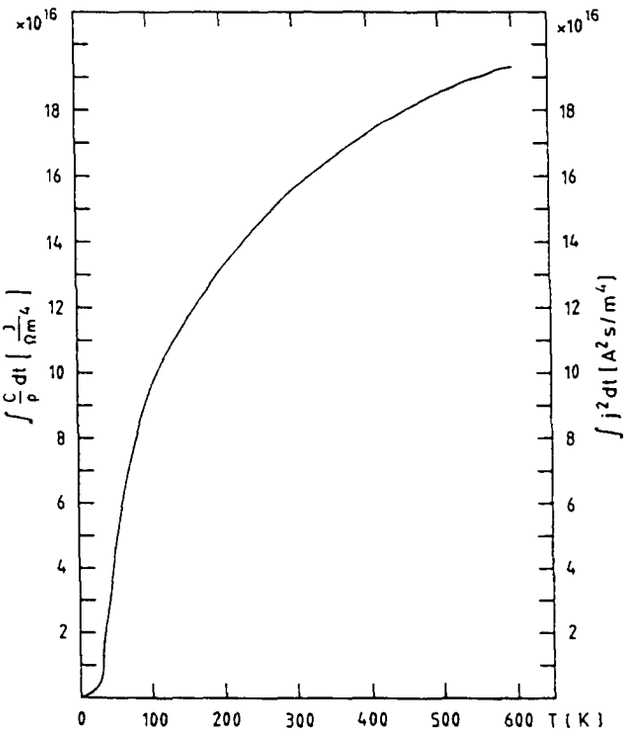

Fig. 33 $f(T_{max}) = \int_0^\infty j^2 dt$ for copper

Assume the current in a magnet starts with Io and decreases with time constant τ, q being the effective copper cross section, then

$$\int_0^\infty j^2 dt = \int_0^\infty \frac{I^2}{q^2}dt = \int_0^\infty \frac{I_0^2 e^{-\frac{2t}{\tau}}}{q^2}dt = \frac{I_0^2 \tau}{2q^2}. \tag{47}$$

With this value the temperature T_{max} is obtained from Fig. 33. T_{max} should be below 500 K.

In the HERA magnets there is a forward and return bus bar running along the outside of the magnet yoke. Here, for the hot-spot temperature, the same consideration as above applies.

During a quench the quenching coils or groups of coils must be protected by bypassing the main current around them. This is done by either cold diodes at each magnet (HERA) or warm diodes at groups of magnets (TEVATRON, SSC). Warm diodes require that safety current leads pass from the coils to the room-temperature diodes at regular intervals along the magnet string.

Voltage taps at main coils are required for quench detection. Usually there is a centre tap at each coil in order to achieve high sensitivity by balancing the half coils.

Quench heaters (HERA: stainless steel strips) may be necessary to distribute the quenching zone over the whole length of the magnet in order to limit the hot-spot temperature.

During a quench high voltages, which may be between 500 V and 1 kV, occur at a magnet or magnet string. The coil insulation must stand these voltages safely. Therefore, a test voltage of about 5 kV to ground in dry air is applied.

The most critical points are the electrical feedthroughs at the warm side with 2 - 3 bar helium gas pressure inside and air outside. One must take into account that the electrical breakdown voltage in 1 bar helium is about a factor 10 lower than in air. Therefore at 1 bar 5 kV in air is equivalent to 0.5 kV in helium.

Appropriate insulation material is Kapton or glass-Kapton-glass composite tape, Tefzel and PEEK (polyether-etherketone). All these materials are good both for cryogenic and high radiation dose applications. Temperature sensors such as platinum or carbon resistors are frequently used for diagnosis.

5.5 Cryostat

The cryostat serves to insulate the cold part of the magnet from the room temperature surroundings. The design aims to obtain the lowest possible heat loads and relatively simple support structures.

5.5.1 Helium Vessel

The helium vessel consists of half shells surrounding the yoke, end plates, the beam tube and tubes for the 1-phase and 2-phase helium, all made from stainless steel.

The half shells are longitudinally welded, which, if necessary, allows a curvature to be introduced into the cold mass. The welding can be used to pretension the yoke/coil structure (RHIC, SSC). For the HERA dipoles the yoke end plates are welded to the inside of the half tubes in order to prevent the longitudinal motion of the coil ends. Other designs have bolted structures for retaining the coil ends. At RHIC and SSC dipoles the coil ends are prestrained axially.

Special care must be taken in selecting the material for the beam tube because it is nearest to the good field region. The same criteria apply as were discussed already for the collars. The beam tube may be equipped with correction coils [26] (sextupole, quadrupole, decapole for HERA dipoles, 12-pole for HERA quadrupoles).

The helium vessel end plates are welded to the ends of the half shells. One- and two-phase tubes as well as safety tubes welded to the end plates contain bellows to accommodate thermal expansion. Stainless steel forgings for flanges must be selected carefully so that they do not have microcracks which may result in leaks.

All cold parts are covered with superinsulation consisting of 5 - 10 layers of Mylar aluminised on both sides (0.04 μm thick) in order to reduce heat flow due to thermal radiation.

5.5.2 Vacuum Vessel

The vacuum vessel can be made from stainless steel or from magnetic steel. The latter may be required if additional magnetic shielding is necessary. If the vacuum vessel is made

from magnetic steel, the inner surface is painted with epoxy in order to reduce outgassing of the surface.

5.5.3 Radiation Shield

Heat flow due to thermal radiation from the warm vacuum vessel is reduced by heat intercepts at one or sometimes two intermediate temperature levels. Such radiation shields consist of a tube made from material of good thermal conduction (aluminium or copper) equipped with cooling tubes. The cooling may be achieved with liquid nitrogen or helium gas. If the cooling tubes are made from aluminium, transition pieces to the stainless steel flanges are required. They are made by friction welding.

The radiation shield is covered with many layers of superinsulation. For the HERA magnets there are 30 layers, each consisting of a perforated sheet of Mylar, aluminised on both sides, and a glass-fibre net as spacer. The perforations and the glass-fibre net are chosen to improve pumping. This kind of superinsulation reduces the heat load to about 0.7 W/m^2 between 300 K and 70 K.

It is extremely important that no direct view of the helium vessel is possible through the thermal shield. Each tiny open space would lead to an increased heat load because the radiation of a black radiator between 300 K and 4 K is about 500 W/m^2.

As the radiative loss follows the law

$$\frac{dQ}{dt} \propto \left(T_1^4 - T_2^4\right) \tag{48}$$

the radiation from the shield at 77 K (T_1) to the 4 K (T_2) area is almost negligible. Some magnets are built with an additional second shield (SSC : 20 K, LHC : 5 K).

5.5.4 Supports

To support the cold mass inside the vacuum vessel several approaches have been used.

In the TEVATRON magnets [4] a structure of glass-fibre epoxy blocks has been used with a 77 K liquid nitrogen temperature intercept. As the thickness of the blocks is small because of the limited space, the heat load through them is rather high. The positioning of the supports in this case must be very accurate as an off-centring of the warm yoke would introduce not only forces but also quadrupole harmonic field distortions. The effect of thermal shrinkage is compensated by using so-called "smart bolts" (spring loaded bolts) for the upper supports.

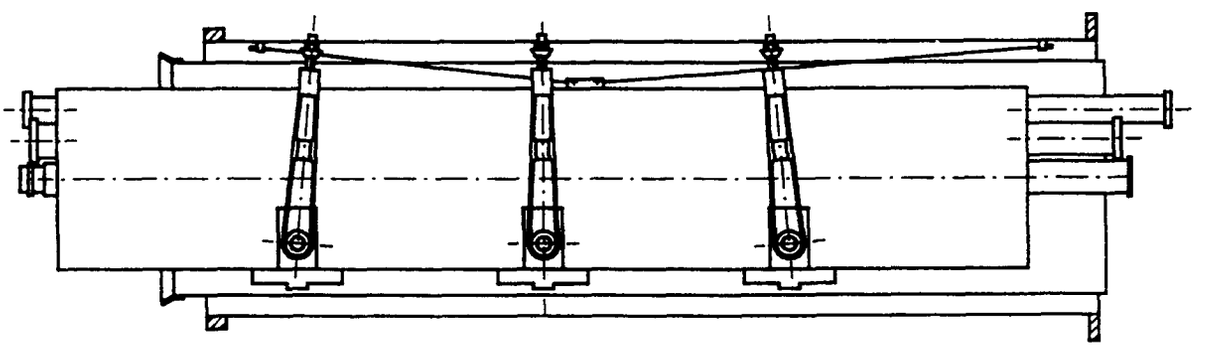

Fig. 34 Support system of HERA dipoles

For cold-yoke magnets like at HERA and UNK a system of transversal rods and vertical bands (belts) or rods is used. For HERA there are such support systems at three longitudinal positions (Fig. 34). The transversal rods are made from glass-fibre epoxy, the belts from unidirectional glass-fibre impregnated with epoxy. At UNK the vertical and horizontal supports are made from titanium.

The advantage of these support systems is relatively low heat loads because of the space available. A certain disadvantage is the fact that many penetrations through the radiation shield must be closed carefully.

A different system is used for SSC and RHIC and is planned for LHC magnets. At SSC magnets re-entrant fibre-reinforced epoxy cylinders are used as support posts (Fig. 35). At RHIC and LHC similar but straight posts are used. RHIC posts are injection-moulded. There is only one hole in the thermal shield from the bottom of the magnet for each support. The thermal intercepts at shield temperature are relatively easy to arrange. Such systems, therefore, lead to the lowest heat loads known so far.

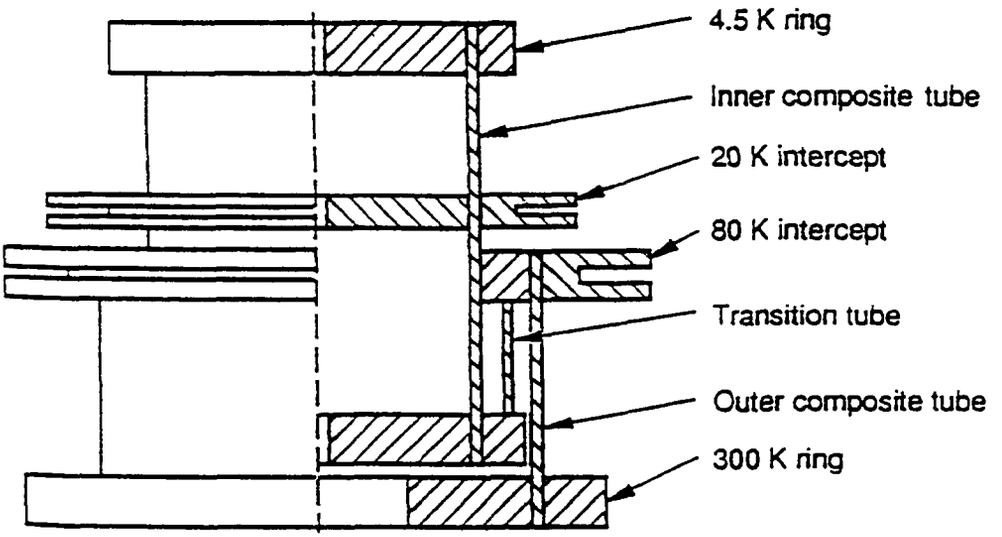

Fig. 35 SSC dipole support post

6. TEST RESULTS AT HERA MASS PRODUCTION MAGNETS

A total of 445 HERA standard dipoles of 9.7 m length, 8 vertical deflecting dipoles of reduced length and 246 HERA quadrupoles of various types have been built, many also containing correction coils or correction magnets. All magnets have been tested cryogenically.

The magnets have been fabricated at several industrial firms:

Dipoles at ANSALDO/ZANON (A/Z) and ABB,
quadrupoles at ALSTHOM and KWU/NOELL,
correction coils at HOLEC and NOELL.

Superconducting cable for these magnets was produced by Europametalli - LMI and by the Swiss Superconductor Consortium (leadership ABB) for dipoles, and at Vacuumschmelze for quadrupoles.

The experience with the industrial fabrication of these superconducting magnets was very good [27]. Many data were collected during magnet testing showing the excellent performance [28]. A brief summary of the results is given here.

6.1 Quench Behaviour

Dipoles and quadrupoles have been quenched at about 4.75 K several times. There is only negligible training, i.e. saturation of the quench current at constant temperature is reached immediately after one or two quenches (Fig. 36).

Average maximum quench current for the dipoles is about 6500 A, however, with two peaks, that of the Italian dipoles being a little lower and with wider distribution (Fig. 37). The reason is the performance of the cable.

The quench current of the quadrupole is considerably higher (Fig. 38).

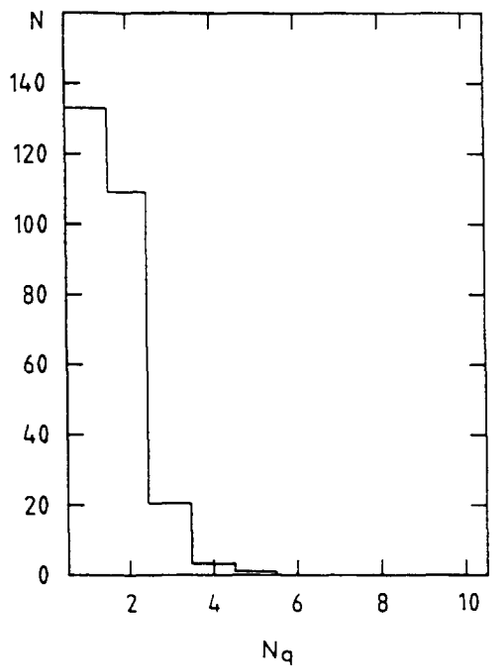

Fig. 36 Number of quenches to reach maximum quench current of HERA dipoles

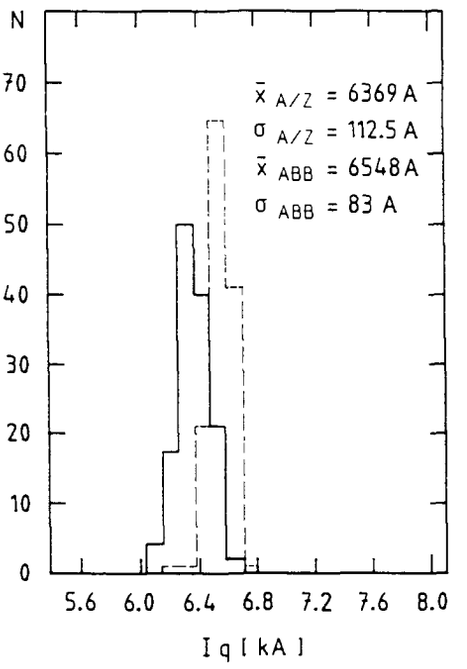

Fig. 37 Statistics of maximum quench current for German (ABB, dashed curve) and Italian (A/Z, solid curve) HERA dipoles

6.2 Field Quality

The normalised field integral ($\int Bdl/I$) in the dipoles shows two peaks differing by about 2 ‰, with the ABB magnets on the high side (Fig. 39). The reason must be the different tooling used by the firms which results in different radii of the coil and in slightly different coil lengths.

The field quality expressed in harmonic coefficients at 5000 A is very good (Fig. 40). Some larger spread in the measurements of the sextupole (b_3) and the skew quadrupole (a_2) reflect the limited accuracy in the arc length of the coil and the difficulty in fixing the mid plane between the half coils.

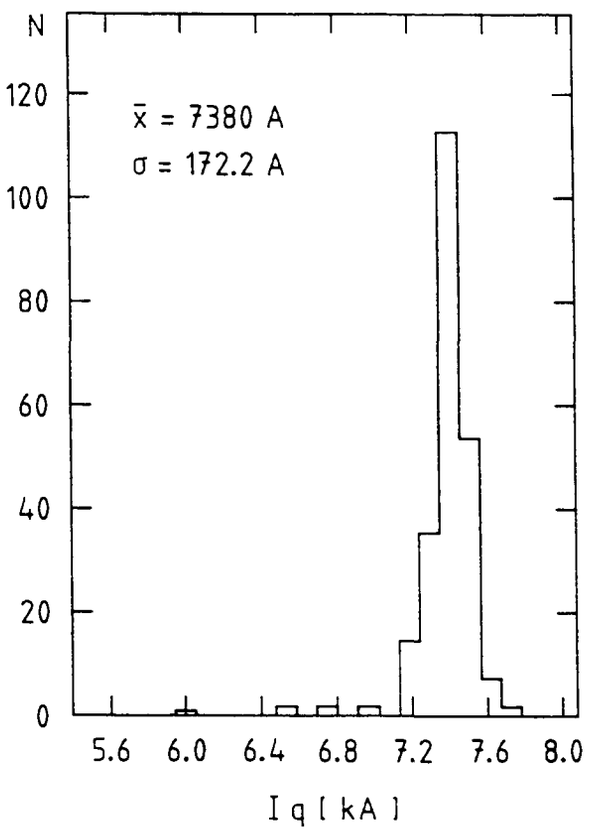

Fig. 38 Statistics of maximum quench current for HERA quadrupoles

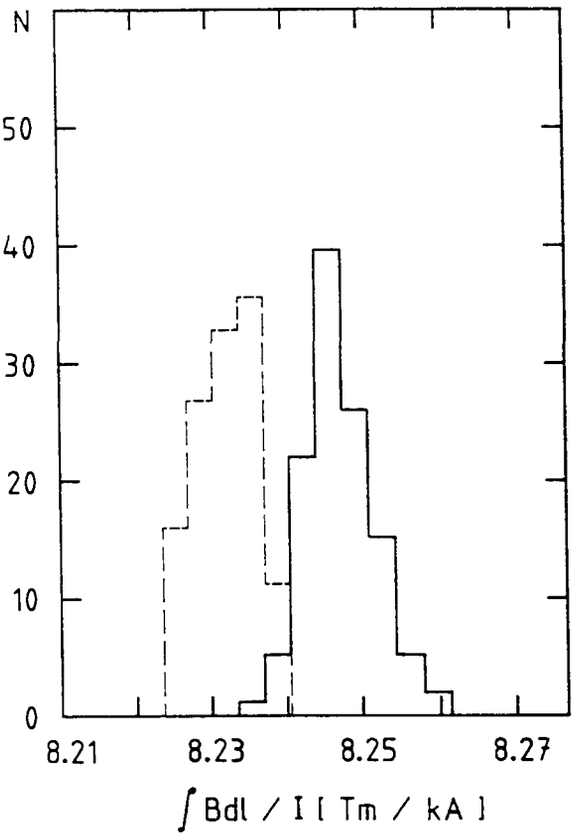

Fig. 39 ∫Bdl/I at 2100 A for HERA dipoles, German magnets (ABB, solid curve), Italian magnets (A/Z, dashed curve).

The correlation between cold measurements at 5000 A and warm measurements at a few amperes for collared coils is generally good (Fig. 41).

As has been explained earlier, in the dipoles there are sextupole and decapole coefficients of considerable strength at low currents and which are the result of inducing currents in the superconducting filaments during current ramping (see Fig. 16). This results in the need to have sextupole and decapole correction coils.

At injection (250 A) there is also a time dependence of the sextupole (and also decapole) component as indicated in Fig. 42 [29]. Here the harmonic coefficient is plotted versus the logarithm of time. A certain linearity in this plot is visible. This indicates that a fraction of the time dependence results from a phenomenon known as flux creep.

The time dependence is different for cables from different firms (Fig. 43). It also depends on the current ramping history of the magnet.

Figure 44 shows that a current cycle with a lower maximum current has a smaller time dependence. This effect allows the bad influence of the changing b_3 at injection to be minimised by appropriate current ramp cycles. Another sensitive parameter for hysteresis is the temperature of the dipole coils (Fig. 45) [13]. For the quadrupoles similar field results are obtained. Here, however, the 12-pole and the 20-pole are the ones which show persistent current effects.

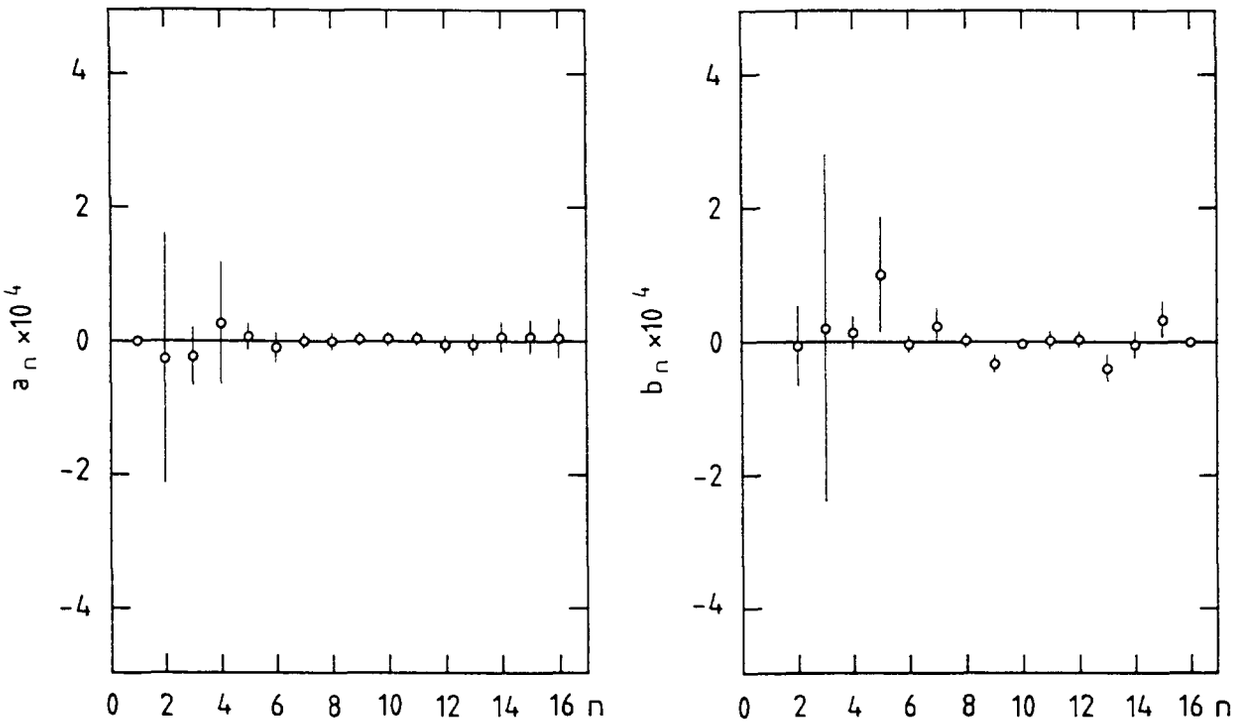

Fig. 40 Skew (a_n) and normal (b_n) harmonic coefficients measured at HERA dipole at 5000A

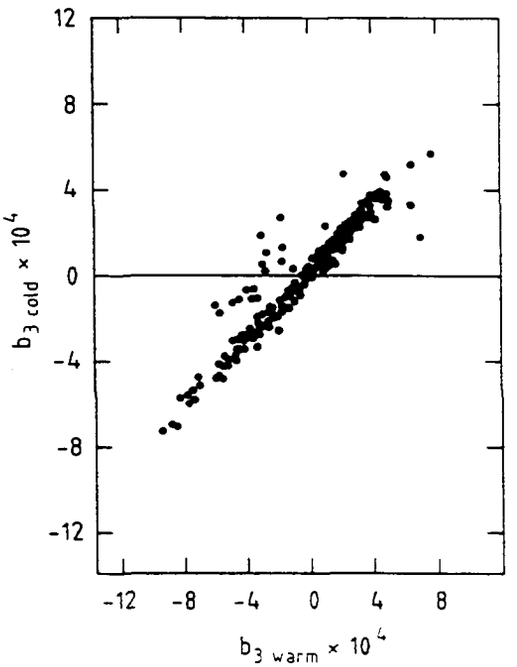

Fig. 41 Correlation between cold (5000 A) and warm b_3 measurements for HERA dipoles

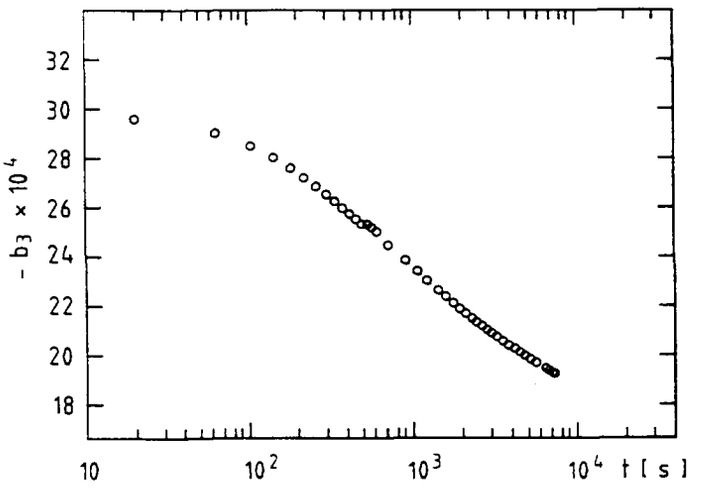

Fig. 42 Time dependence of sextupole harmonic coefficient at injection

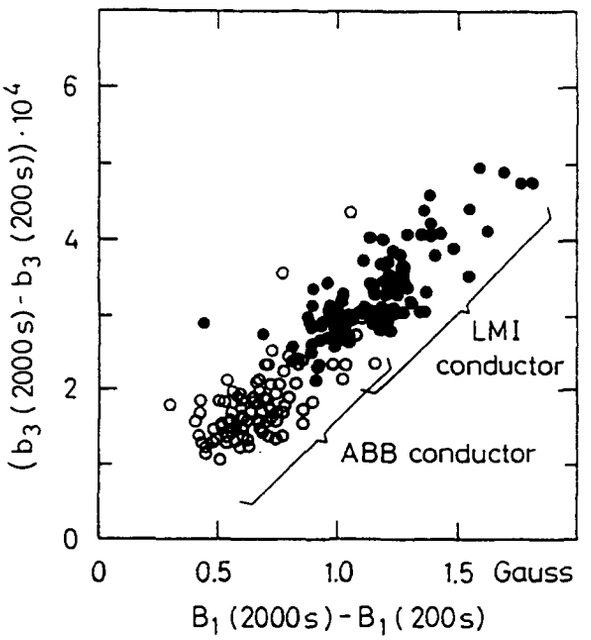

Fig. 43 Correlation between the logarithmic decay rates of the sextupole and dipole components in HERA dipoles (one initial cycle with I_{max} = 6000 A) [29]

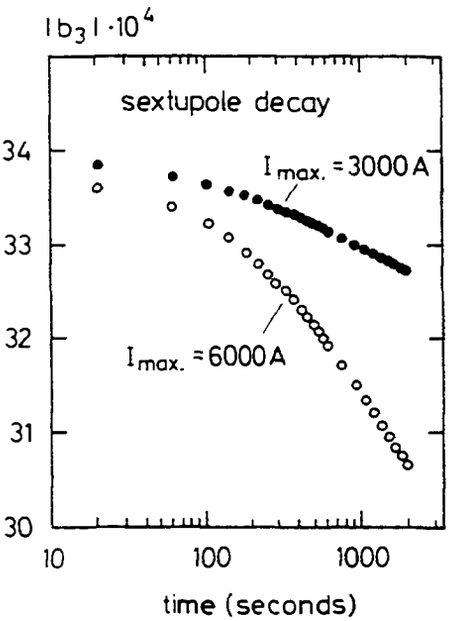

Fig. 44 Time dependence of the sextupole coefficient at a dipole current of 250 A [29], curve (a): I_{max} = 6000 A, curve (b): I_{max} = 3000 A

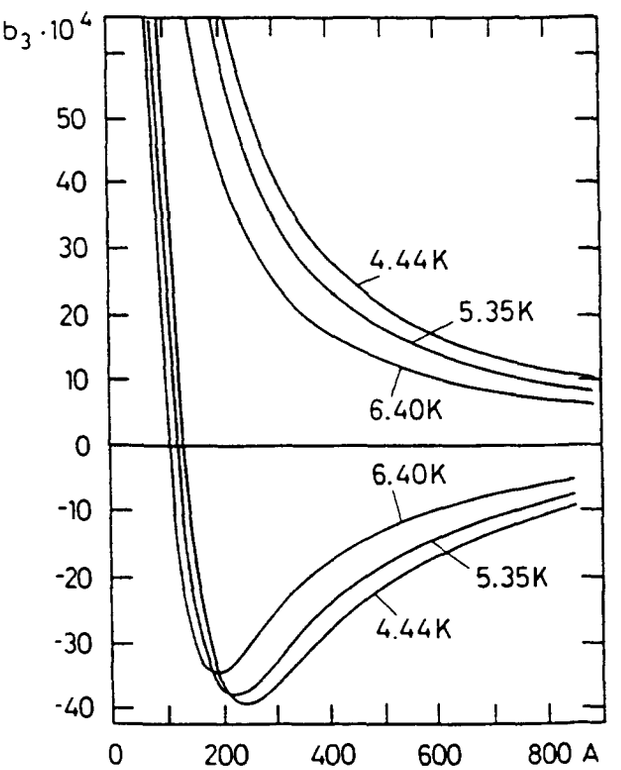

Fig. 45 Sextupole hysteresis in a HERA dipole magnet with LMI conductor for different temperatures [13]

The distributed sextupole and quadrupole correction coils inside the dipoles lead to a coupling of the persistent current field effects and non-negligible field distributions in these magnets [30].

When measured along the dipole axis the persistent current fields exhibit a variation with a wave length corresponding to the cable twist pitch length Fig. 46 [31]. This indicates a non-uniform current distribution in the cable. The reason for this phenomenon may be the different critical quench currents of the strands and/or the structure of the cable splices.

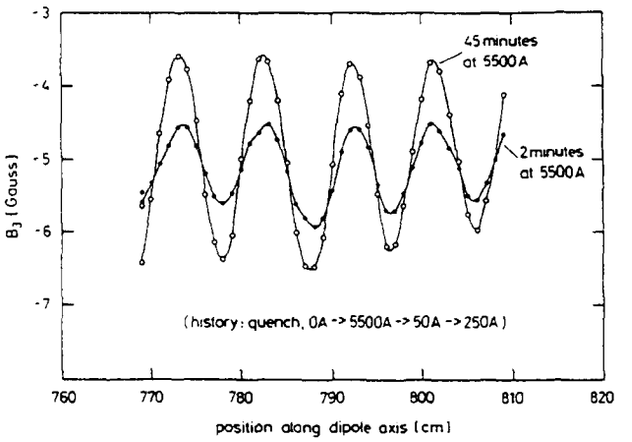

Fig. 46 Sextupole field along the axis of an ABB dipole measured at 250 A after a single cycle to 5500 A with 2 minutes respectively 45 minutes waiting time at 5500 A

7. CONCLUSIONS

The experience with present superconducting magnets shows that the design of such magnets is fully understood and that they can be built in large quantities by industry with good quality. With NbTi superconductors fields of about 6 Tesla at 4.6 K are easily reached. The necessary structural and insulating materials suitable for low temperature and for high radiation dose level are available. Many elaborate design tools in the form of finite element and field programs including saturation exist.

The achieved field quality is fully sufficient for accelerator operation. Static and dynamic field distortions at injection fields can be compensated by suitable correction magnets.

REFERENCES

[1] H. Brechna, Superconducting Magnet Systems, Springer Verlag, Berlin 1973

[2] K.-H. Meß and P. Schmüser, CERN Accelerator School, Superconductivity in Particle Accelerators, CERN 89-04, March 1989, p. 87, P. Schmüser, private communication

[3] M. N. Wilson, Superconducting Magnets, Clarendon Press, Oxford 1983

[4] F. T. Cole et al., editors, A Report on the Design of the FNAL Superconducting Accelerator, May 1979, final magnet cross section received from J. Carson, Fermilab, private communication

[5] HERA, A Proposal for a Large Electron-Proton Colliding Beam Facility at DESY, DESY HERA 81-10, 1981

[6] S. Wolff, Superconducting Magnets for HERA, Proceedings of the XIII International Conference on High Energy Particle Accelerators, Novosibirsk, Aug. 1986, Vol. 2, p. 29, DESY HERA 1986-12

[7] H. Kaiser, Design of Superconducting Dipole for HERA, Proceedings of the XIII International Conference on High Energy Particle Accelerators, Novosibirsk, Aug. 1986, Vol. 2, p. 49, DESY HERA 1986-14

[8] Conceptual Design of the Relativistic Heavy Ion Collider, RHIC, Report No. BNL51932, Brookhaven National Laboratory, Upton N. Y. 1986, latest version of magnet design received from A. Greene, BNL, private communication

[9] Conceptual Design of the Superconducting Supercollider, SSC Central Design Group, Lawrence Berkeley Laboratory, CDG SSC-SR-2020, March 1986, and, Superconducting Super Collider Site-Specific Conceptual Design, SSC Laboratory, SSC-SR-1051, June 1990, latest version of magnet design received from C. L. Goodzeit, SSCL, private communication

[10] G. Brianti and K. Hubner (Eds.), The Large Hadron Collider in the LEP Tunnel, CERN-87-05, May 1987, latest version of magnet design received from R. Perrin, CERN, private communication

[11] R. Auzolle et al., First Industry Made Superconducting Quadrupoles for HERA, Proceedings of the Applied Superconductivity Conference, San Francisco, 1988, IEEE Transactions on Magnetics, Vol. 25, 1989, p. 1660

[12] A. Asner, R. Perrin, S. Wenger, F. Zerobin, First Nb_3Sn 1 m Long Superconducting Dipole Model Magnets for LHC Break the 10 Tesla Field Threshold, Proceedings of the 11^{th} International Conference on Magnet Technology, Tsukuba, Japan, 1989, p. 36

[13] H. Brück et al., Persistent Current Effects in the Superconducting HERA Magnets and Correction Coils, Proceedings of 2^{nd} European Particle Accelerator Conference, Nice, June 1990, Vol. 2, p. 1160

[14] E. W. Collings, M. D. Sumption, Innovative Strand Design for Accelerator Magnets, XV^{th} International Conference on High Energy Accelerators, Hamburg, July 1992

[15] H. Hirabayashi, et. al., Design Study of a Superconducting Dipole Model Magnet for the Large Hadron Collider, IEEE Transactions on Magnetics, Vol. 27, No. 2, 1991, p. 2004

[16] J. Strait, SSCL, private communication

[17] K. Balewski, Untersuchung der Feldqualität supraleitender Dipolmagnete, Diplomarbeit, Hamburg University 1985

[18] D. Larbalestier, Selection of Stainless Steel for the Fermilab Energy Doubler/Saver Magnets, TM-745 1630.000, Fermilab, October 1977

[19] J. Perot, CEN-Saclay, private communication

[20] G. Meyer, DESY, private communication

[21] M. D. Anarella, R. Jackimowicz, The Application of Strain Gauges for Measuring Coil Stresses in HERA Dipole Magnets at DESY/Results of Coil Stress Measurements on a 1 m HERA Magnet at DESY, AD/SSC/Techn. No. 63 SSC-N-378, Brookhaven National Laboratory, August 20, 1987

[22] T. Ogitsu, et. al., Mechanical Performance of 5-cm-Aperture, 15-m-Long SSC Dipole Magnet Prototypes, Proceedings of the 1992 Applied Superconducting Conference, Chicago

[23] A. F. Greene and E. Willen, private communication

[24] K. Sinram, The Influence of Fine Blanking on the Magnetic Properties of Soft Magnetic Steel, Proceedings of the 10th International Conference on Magnet Technology, Boston, September 1987, IEEE Transactions on Magnetics, Vol. 24, 1988, p. 839

[25] C. L. Goodzeit, private communication

[26] C. Daum et al., The Superconducting Quadrupole and Sextupole Correction Coils for the HERA Proton Ring, DESY HERA 89-09, Feb. 1989

[27] E. Apostolescu, et. al., Summary of Experience with Industrial Superconducting Magnet Production for HERA, IEEE Transactions on Magnetics, Vol. 28, No. 2, 1992, p. 689

[28] H. R. Barton et al., Performance of the Superconducting Magnets for the HERA Accelerator. Proceedings of the 11th International Conference on Magnet Technology, Tsukuba, Japan, 1989, p. 147

R. Meinke, Superconducting Magnet System for HERA, IEEE Transactions on Magnetics, Vol. 27, No. 2, 1991, p. 1728

P. Schmüser, Field Quality Issues in Superconducting Magnets, Conference Record of the 1991 IEEE Particle Accelerator Conference, Vol. 1, 1991, p. 37

P. Schmüser, Magnetic Measurements of Superconducting Magnets and Analysis of Systematic Errors, CERN Accelerator School, Montreux, March 1992, CERN 92-05, p. 240

[29] H. Brück et al., Time Dependence of Persistent Current Field Distortions in the Superconducting HERA Magnets, Proceedings of 2nd European Particle Accelerator Conference, Nice, June 1990, Vol. 1, p. 329

[30] M. Pekeler, et. al., Coupled Persistent Current Effects in the HERA Dipoles and Beam Pipe Correction Coils, Proceedings of the 3rd European Particle Accelerator Conference, Berlin, 1992

[31] H. Brück, et. al., Observation of a Periodic Pattern in the Persistent-Current Fields of the Superconducting HERA Dipole Magnets, DESY HERA 91-01 (1991)